Lithos 296–299 (2018) 281–296

Contents lists available at ScienceDirect

Lithos

journal homepage: www.elsevier.com/locate/lithos

Slab break-off triggered lithosphere - asthenosphere interaction at a convergent margin: The Neoproterozoic bimodal magmatism in NW India

Wei Wang [a,*], Manoj K. Pandit [b], Jun-Hong Zhao [a], Wei-Terry Chen [c], Jian-Ping Zheng [a]

[a] State Key Laboratory of Geological Processes and Mineral Resources, School of Earth Sciences, China University of Geosciences, Wuhan 430074, China
[b] Department of Geology, University of Rajasthan, Jaipur 302004, Rajasthan, India
[c] State Key Laboratory of Ore Deposit Geochemistry, Institute of Geochemistry, Chinese Academy of Sciences, Guiyang 550002, China

ARTICLE INFO

Article history:
Received 16 July 2017
Accepted 8 November 2017
Available online 12 November 2017

Keywords:
E-MORB and OIB like basalt
Lithosphere-asthenosphere interaction
Slab window
Malani Igneous Suite
NW India
Rodinia

ABSTRACT

The Neoproterozoic Malani Igneous Suite (MIS) is described as the largest felsic igneous province in India. The linearly distributed Sindreth and Punagarh basins located along eastern margin of this province represent the only site of bimodal volcanism and associated clastic sediments within the MIS. The in-situ zircon U-Pb dating by LA-ICPMS reveals that the Sindreth rhyolites were erupted at 769–762 Ma. Basaltic rocks from both the basins show distinct geochemical signatures that suggest an *E*-MORB source for Punagarh basalts (low Ti/V ratios of 40.9–28.2) and an OIB source (high Ti/V ratios of 285–47.6) for Sindreth basalts. In the absence of any evidence of notable crustal contamination, these features indicate heterogeneous mantle sources for them. The low $(La/Yb)_{CN}$ (9.34–2.10) and Sm/Yb (2.88–1.08) ratios of Punagarh basalts suggest a spinel facies, relatively shallow level mantle source as compared to a deeper source for Sindreth basalts, as suggested by high $(La/Yb)_{CN}$ (7.24–5.24) and Sm/Yb (2.79–2.13) ratios. Decompression melting of an upwelling sub-slab asthenosphere through slab window seems to be the most plausible mechanism to explain the geochemical characteristics. Besides, the associated felsic volcanics show A_2-type granite signatures, such as high Y/Nb (5.97–1.55) and Yb/Ta (9.36–2.57) ratios, consistent with magma derived from continental crust that has been through a cycle of continent-continent collision or an island-arc setting. A localized extension within an overall convergent scenario is interpreted for Sindreth and Punagarh volcanics. This general convergent setting is consistent with the previously proposed Andean-type continental margin for NW Indian block, the Seychelles and Madagascar, all of which lay either at the periphery of Rodinia supercontinent or slightly off the Supercontinent.

1. Introduction

The Neoproterozoic Era has been hailed as one of the most dynamic periods in the history of the Earth on account of large-scale crustal growth, increased latitudinal velocities of crustal blocks and consequent rapid shift in their spatial positions (Hoffman et al., 1998; Li et al., 2013; McCall, 2006; Meert and Lieberman, 2008; Shields, 2007). Significant modifications in the atmospheric composition during this time period paved way for the ensuing explosion of life during Cambrian. This time window also coincides with the final assembly and break-up of the supercontinent Rodinia and has evoked geoscientific attention on multitude of aspects, such as its formation, position and mutual relationship of constituent continental blocks and its break up (Evans, 2013; Hoffman, 1991; Li et al., 2008; Moores, 1991; Nance et al., 2014). Despite geochemical, structural and geochemical data and reliable U-Pb ages made available from various crustal components of Rodinia as a consequence of such efforts, its configuration and latitudinal position of constituent continental blocks as well as the timing of formation and dispersal of the Supercontinent continue to be debated (Cawood et al., 2017; Li et al., 2008; Merdith et al., 2017; Spencer et al., 2013).

The Neoproterozoic age Malani Igneous Suite (MIS) in NW India, on account of suitability of rock types (felsic volcanics, mafic dykes and granite intrusions, etc.) and key location in Rodinia assembly, has been the focus of several paleomagnetic, geochemical, geochronologic and structural studies in the recent years (Torsvik et al., 2001b; Gregory et al., 2009; de Wall et al., 2012; Ashwal et al., 2013; Meert et al., 2013; de Wall et al., 2017). The findings have contributed significantly in refining our understanding on the Neoproterozoic geodynamics of NW Indian block and its paleoposition in the Rodinia supercontinent (Ashwal et al., 2013; Collins et al., 2014; Meert et al., 2013; Merdith et al., 2017). However, the myriad of models on petrogenesis and tectonic setting of MIS, based entirely on the felsic

* Corresponding author.
E-mail address: wwz@cug.edu.cn (W. Wang).

https://doi.org/10.1016/j.lithos.2017.11.010
0024-4937/

component, are diverse and contradictory. These include, a plume setting (Kochhar, 1984), Andean type arc setting (Ashwal et al., 2002), anorogenic extension setting (Bhushan, 2000; Eby and Kochhar, 1990; Sharma, 2004) and mantle demanination (Vijaya Rao and Krishna, 2013). For a long time the MIS was considered as an essentially terrestrial suite of undeformed volcanic and plutonic rocks (Bhushan, 2000; Pareek, 1981; Sharma, 2004). However, variably deformed bimodal volcaniclastic rocks in linear Sindreth and Punagarh basins have recently been included in the ambit of the MIS on account of coeval ages and geochemical similarity (Ashwal et al., 2013; de Wall et al., 2012; Dharma Rao et al., 2012; van Lente et al., 2009). Based on lithoassemblages and alteration features, van Lente et al. (2009) suggested a back-arc setting for these basins while Dharma Rao et al. (2012) favor an ocean floor set up for Sindreth Basin. In a more recent study, Schöbel et al. (2017) have suggested continental faulting and half graben setting for the Sindreth Basin. Significance of mafic rocks and bimodal volcanism in this basis necessitate a detailed attention in understanding petrogenesis and tectonic setting of the MIS and implications on regional geodynamics, especially for Rodinia fragmentation. In this study we present geochemical characteristics of Sindreth and Punagarh bimodal volcanics and zircon U-Pb ages of their felsic components. The findings are discussed in terms of tectonic setting for the MIS magmatism to constrain an overall convergent setting wherein asthenosphere-lithosphere-slab melt interaction was prompted by the formation of a slab window. Heterogeneous mantle sources with both *E*-MORB and OIB components have been inferred for these basins and paleoposition of the NW India in the Rodinia supercontinent has been evaluated in the light of geochemical and isotopic data.

2. Geological setting

2.1. Geological overview of NW Indian block

Precambrian geology of the Indian peninsular region has evolved around four major Archean - Proterozoic cratonic nuclei, namely the Bundelkhand - Banded Gneiss Complex (BGC), the Bastar, Singhbhum and Dharwar cratons, which were stabilized by end-Archean (Fig. 1a)(Meert and Pandit, 2015). The northernmost cratonic nuclei, the BGC (also referred to as the Aravalli Craton) comprises a Paleo-to-Neoarchean basement (~3.3–2.5 Ga) of migmatitic gneisses, granitoids and minor metavolanic and metasedimentary units (Roy and Kröner, 1996; Sinha-Roy et al., 1998; Wiedenbeck and Goswami, 1994). This is overlain by two Proterozoic metasedimentary successions, the Paleoproterozoic Aravalli and Paleo- to Mesoproterozoic Delhi supergroups (Gupta, 1997; Wang et al., 2017a) that together constitute the ~750 km long, NE-trending Aravalli-Dehli Fold Belt (ADFB) having a complex deformation history. The ADFB, together with the BGC, is separated from the Bundelkhand Craton by the Great Boundary Fault. The southern contact is largely concealed under the end Cretaceous Deccan basalts.

The Neoproterozoic events in the NW Indian block begin with ~1 Ga eastward convergence and collision of the Marwar block in the west and ADFB in the east, as recorded by the 990–970 Ma calc-alkaline felsic igneous rocks and associated mafic intrusions along the western margin of ADFB (Deb et al., 2001; Pandit et al., 2003). After a quiescence of ~100 Ma, several granitoid intrusions occurred to the west of southern margin ADFB during 870 to 800 Ma, collectively designated as 'Erinpura Granite' (Choudhary et al., 1984; Heron, 1953; Just et al., 2011; Solanki, 2011). A younger, more extensive, predominantly subaerial, undeformed and unmetamorphosed suite of magmatic rocks, in the region further west, has been described as the Malani Igneous Suite (MIS; Pareek, 1981). The MIS is predominantly felsic in compositions and dated to 770–750 Ma (Gregory et al., 2009; Meert et al., 2013; T.H. Torsvik et al., 2001; Wang et al., 2017b). Till recently the bimodal volcano-clastic sequences in Sindreth and Punagarh basins were not considered as part of the Malani magmatism. However, the more recent geochemical and geochronologic studies clearly implicate inclusion of Punagarh and Sindreth sequences within the framework of MIS (van Lente et al., 2009, Dharma Rao et al., 2012, present study). Variably deformed granitoids of Mt. Abu were earlier described as 'late' phase

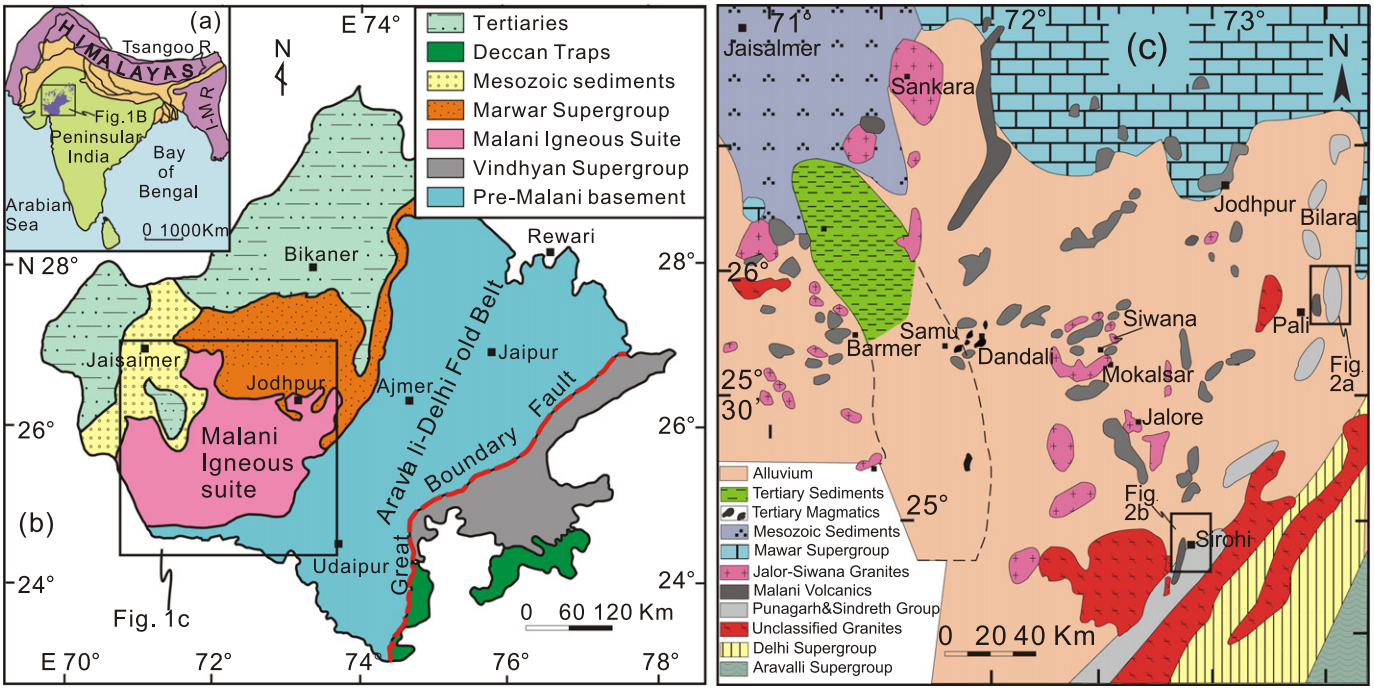

Fig. 1. (a) Geological framework of the Peninsular Indian and adjacent area; I-M R: Indo-Myanmar Range; (b) Pre-quaternary interpretative geological map of Rajasthan of northwestern India, showing the extent of Malani Igneous Suite (adapted from Pareek, 1981). The pre-Malani basement to the east refers to the Delhi and Aravalli supracrustal sequences and underlying Archean complex; (c)The outcrop pattern of the extrusive and intrusive phases of the Malani Igneous Suite (adapted from Roy and Jakhar, 2002). The Pentagram with number represents the location of sampling for geochronolgy. 1: Jodhpur rhyolite; 2: Punagarh dacite; 3: Sindreth rhyolite.

of Erinpura Granite (Heron, 1953), however, geochemical and geochronologic findings (Ashwal et al., 2013; de Wall et al., 2012) establish a Malani affinity for these granitoids too.

2.2. The Sindreth and Punagarh basins

Sindreth and Punagarh basins are approximately NNE - SSW trending elongated to oval structures along the western margin of ADFB with an areal extent of ~40 and 150 km^2, respectively (Fig. 2). Both the basin sequences exhibit common deformation geometry (synclinal structures), no sign of metamorphism but significant alteration (Chore and Mohanty, 1998; van Lente et al., 2009). Sedimentary lithologies in these basins are shale, slate, phyllite, micaceous schist, quartzite and conglomerate (Chore and Mohanty, 1998, Schöbel et al., 2017). Bimodal volcanics with predominant basic and subordinate felsic components are sandwiched between the clastic units in both the basins. The Punagarh rocks unconformably overlie the Sojat Formation and are further subdivided into Bambholai, Khambal and Sowaniya formations from base upwards (Chore and Mohanty, 1998). The Bambholai Formation comprises pillow basalts and interlayered shale and quartzite beds. The Khambal Formation directly overlies the Sojat Formation; the contact exposed only on the eastern limb of the Punagarh Basin. Bedded chert and vesicular and amygdaloidal volcanic rocks were deposited over the quartzite (Fig. 3a). The Sowaniya Formation consists of repetitive felsic and basic flows, and an upper shale – quartzite unit, resting over the volcanics of Khambal Formation (Chore and Mohanty, 1998). The Punagarh dacite consists of K-feldspar and plagioclase phenocrysts, quartz, Fe - Ti oxides and chlorite, and a fine-grained ground mass of quartz, feldspar and amphibole (Fig. 3b).

The Sindreth sediments unconformably overlie the Sirohi Group and have been subdivided into the Khamabal and Angor formations (Chore and Mohanty, 1998). The Khambal Formation mainly comprises unsorted polymictic conglomerate (fanglomerite/debris flow deposit), basalts, rhyolite, bedded rhyolitic tuff and arkose (Fig. 3c). Basalt is variably altered, as seen in replacement of primary plagioclase and clinopyroxene by albite-rich compositions and chlorite, respectively (Fig. 3d). The Angor Formation mainly contains felsic volcanic rocks and bedded mudstone, silicic tuffs and conglomerate. The latter lithology, restricted to the N-S trending ridges, represent basal part of the Formation (Fig. 3e)(Chore and Mohanty, 1998). In a more recent study, Schöbel et al. (2017) have refuted the ocean basin setting for Sindreth rocks and have subdivided Sindreth Basin into lower and upper clastic units, separated by an intervening bimodal volcanic unit. The Sindreth rhyolite has porphyritic texture with phenocrysts of tabular plagioclase, K-feldspar and embayed quartz (Fig. 3f). The groundmass is fine-grained, either glassy and devitrified or composed of quartz, feldspar and amphibole (Fig. 3f). The Sindreth and Sirohi Group sediments as well as the basal Erinpura Granites are crosscut by several WNW to N-S trending dolerite dykes that represent the terminal phase of Malani magmatism in this region (Chore and Mohanty, 1998; Sharma, 2004).

3. Sampling and analytical methods

Two rhyolite samples from the Sindreth Basin were selected for in-situ zircon U-Pb dating, while twenty six whole rock samples, including five Sindreth basalt, seven Sindreth rhyolite, seven Punagarh dacite and seven rhyolite from Jodhpur region were analyzed for whole rock elemental and isotopic analyses.

3.1. In situ zircon U-Pb analyses

Approximately 2 kg of sample was crushed for standard heavy mineral separation procedures. Morphology and internal structure of zircon separates from the bulk were observed using a Gatan Mono CL 4+ detector attached to a Zeiss Sigma 300 field emission SEM, at the State Key Laboratory of Geological Processes and Mineral Resources (SKLGPM), China University of Geosciences, Wuhan. Selected zircons

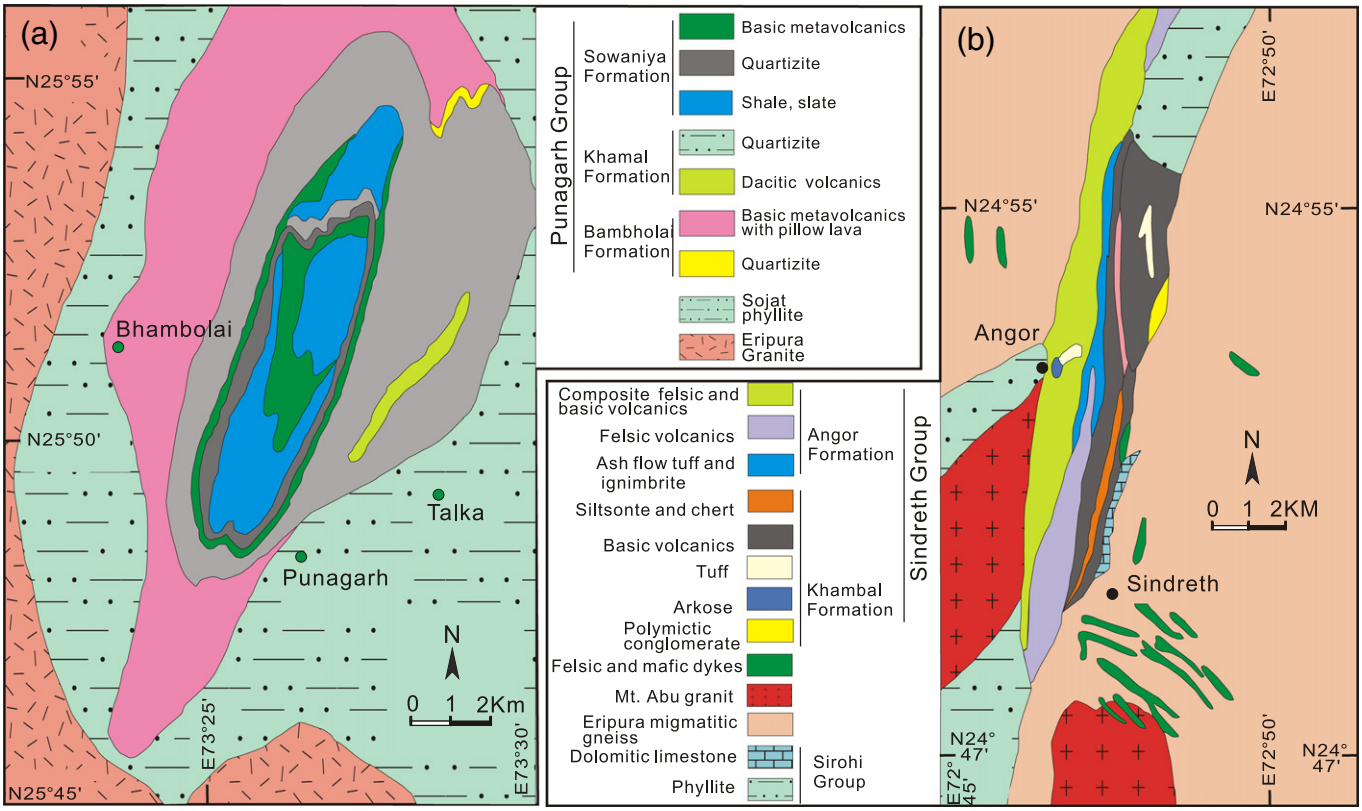

Fig. 2. Geological map showing distribution of the Sindreth and Punagarh volcano-sedimentary sequences, modified from Chore and Mohanty (1998) and van Lente et al. (2009).

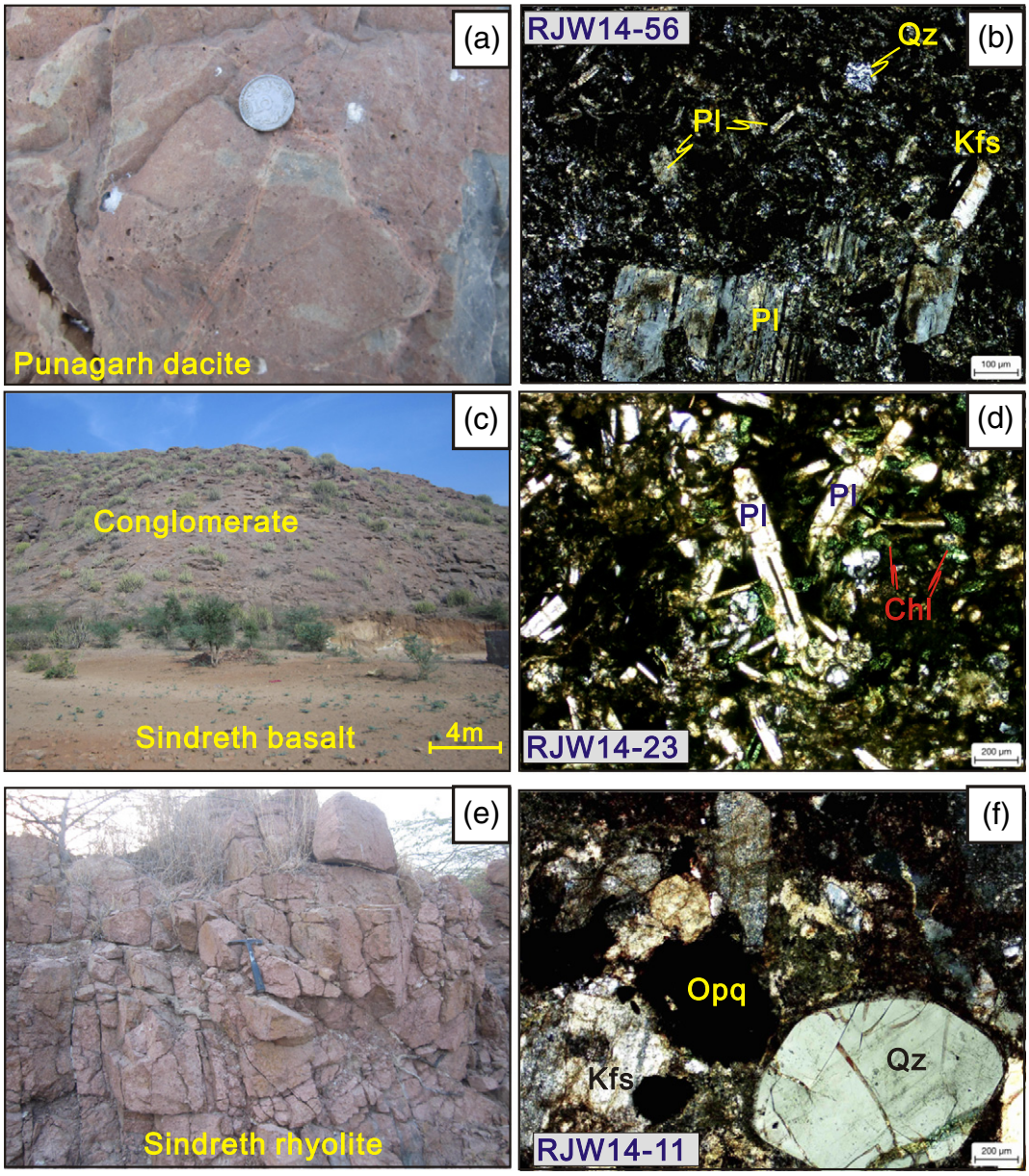

Fig. 3. Photographs and photomicrographs showing features of the studied mafic and felsic volcanic rocks. (a) Punagarh dacite with vesicular structure; (b) Plagioclase in the Punagarh dacite showing alteration; (c) The Sindreth conglomerate and basalt that has been largely weathered away; (d) Primary plagioclase and clinopyroxene in the Sindreth basalt, partially replaced by albite and chlorite; (e) Strongly fragmented massive Sindreth rhyolite; (f) Quartz and altered K-feldspar phenocrysts in the Sindreth rhyolite. Abbreviation: Qz-quartz, Pl-plagioclase, Kfs-Potassium feldspar, Chl-chlorite, Opq-opaques.

were subjected to in-situ U-Pb isotopic analyses using an Agilent 7500a Inductively Coupled Plasma Mass Spectrometer (ICPMS), coupled to a 193 nm ArF Excimer Laser ablation system, housed at the Geological Experimental Testing Center of Hubei, China. The Geolas193 nm ArF excimer laser, homogenized by a set of beam delivery systems, was focused on the zircon surface with the fluence of 8 J/cm^2. A spot diameter of 32 μm was ablated at 5 Hz repetition rate for 45 s. Helium (optimized to obtain the highest sensitivity) was applied as a carrier gas to allow efficient transportation of aerosol to the ICP-MS using a 1m transfer tube with an internal diameter of 3 mm. Zircon 91500 was used as the primary standard to correct elemental fractionation. Zircon, GJ-1, was also analyzed as unknown sample for quality control. Raw data reduction was performed off-line by *ICPMSDataCal* (Liu et al., 2010) and the results are reported with 1σ error. Since the net intensities of 204 (Pb + Hg) are lower than 20 cps in most cases, common Pb was not subtracted in this work due to large analytical uncertainty. Data were processed using the ISOPLOT and the DensityPlotter programs (Ludwig, 2003). The metadata of LA-ICPMS U-Pb as well as the results of reference material GJ-1, are presented in Table S1.

3.2. Bulk rock major and trace element analyses

Major element abundances were obtained on fused glass beads by X-ray fluorescence spectrophotometer (XRF) hosted in the SKLGPM. Visibly fresh pieces of rock (~20 g) were crushed to 200-mesh in an alloy mortar. Loss on Ignition (LOI) values were determined on 0.5 g sample powder after heating it to 1000 °C for one-hour. Analyses of international rock standards (BCR-2, GSR-1 and GSR-3) demonstrate precision and accuracy better than 5% for major oxides.

Trace elements, including REE, were analyzed on an Elan DRC-II ICP-MS, at the Laboratory of Radiogenic Isotope Geochemistry, University of Science and Technology of China (USTC). 50 ± 1 mg of sample powder was digested in HF + HNO_3 mix in a teflon bomb at 190 °C for 48 h. The soluble residue was mixed with Rh solution

as internal standard. Pure elemental standards were used for external calibration and BHVO-2, AGV-2 and BCR-2 were used as reference materials. The analytical precision is better than 5% for elements with concentrations higher than 10 ppm, and less than 10% for those with <10 ppm concentration.

3.3. Bulk rock Sr-Nd isotopic analysis

For whole rock Sr-Nd isotopic analysis, ~100 mg sample powder was dissolved in distilled HF + HNO_3 in teflon capsules, and elemental separation was done by conventional cation-exchange techniques (Chen et al., 2002, 2007). Strontium and neodymium were separated and purified on quartz columns by conventional ion exchange chromatography with a 5-ml resin bed of AG 50 W-X12 (200–400 mesh) and HDEHP, di (2-ethylhexyl)orthophosphoric acid after sample dissolution. Isotopic analyses of collected Sr and Nd were performed on a multi-collector Finnigan MAT-262 mass spectrometer in static mode, at the Laboratory for Radiogenic Isotope Geochemistry, USTC. Measured $^{87}Sr/^{86}Sr$ and $^{143}Nd/^{144}Nd$ ratios were corrected for mass fractionation relative to $^{86}Sr/^{88}Sr = 0.1194$ and $^{146}Nd/^{144}Nd = 0.7219$, respectively.

4. Results

The analytical results of U-Pb isotopic, bulk rock elemental and Sr-Nd isotopic analyses are presented in Tables 1, 2 and Table S2.

4.1. In-situ zircon U-Pb ages

Sample RJW1416 is a rhyolite from the Khamal Formation collected from southwest of the Sirohi town. Zircon grains from this sample show a length/width ratio of ~2:1, oscillatory zoning (Fig. 4) and high Th/U ratios of 1.61 to 0.83, all attesting to their magmatic origin. Twelve out of 15 analyses gave $^{206}Pb/^{238}U$ ages between 769.8 ± 12.6 Ma and 756.3 ± 12.9 Ma yielding a weighted mean age of 761.9 ± 6.1 Ma (2σ, MSWD = 0.15), representing the crystallization age of the rhyolite. The other three analyses yield distinctly older $^{206}Pb/^{238}U$ ages that range from 819.3 ± 11.7 Ma to 807.3 ± 13.8 Ma, most likely inherited from the Erinpura Granite basement, which is also evident from their variably rounded and etched morphologicies (Fig. 4).

Sample RJW1418, is a rhyolitic tuff from the overlying Angor Formation, collected from northwest of Sindreth village. Zircon grains from this sample show length/width ratios of ~2:1, oscillatory zoning or homogeneous internal structures (Fig. 4) and high Th/U ratios of 2.14 to 0.91, all indicative of igneous origin. All the 15 analyses yield concordant U-Pb ages, with a weighted mean of 769.0 ± 5.2 Ma (2σ, MSWD = 0.66) that we interpret as the crystallization age of the rhyolite.

The obtained zircon U-Pb ages of 769.0 ± 5.2 Ma and 761.9 ± 6.1 Ma are in perfect agreement with previously reported 767–761 Ma and 768–765 Ma ages for the Sindreth and Punagarh felsic rocks (Dharma Rao et al., 2012; van Lente et al., 2009; Wang et al., 2017b), further substantiating the MIS affinity of Sindreth and Punagarh sequences.

4.2. Bulk rock geochemistry of volcanic rocks

Geochemical characteristics of mafic volcanic rocks from Sindreth and Punagarh basins and rhyolites from Jodhpur area were evaluated, and geochemical dataset of 31 basalt, 3 dacite and 4 rhyolite samples from van Lente et al. (2009) have also been considered for interpretation.

4.2.1. Basalts

The Sindreth and Punagarh basalts share common geochemical signatures, characterized by wide range of SiO_2 (55.4–40.2 wt%), Al_2O_3 (16.8–12.0 wt%), highly variable TiO_2 (3.18–1.96 wt%), $Fe_2O_3^{(T)}$ (19.7–

Table 1
U-Pb isotopic data of zircons from rhyolites from the Sindreth basin.

Spot	Pb	Th	U	$^{207}Pb/^{206}Pb$		$^{207}Pb/^{235}U$		$^{206}Pb/^{238}U$			Th/U	$^{207}Pb/^{206}Pb$		$^{207}Pb/^{235}U$		$^{206}Pb/^{238}U$		Con.(%)[a]
	ppm	ppm	ppm	Ratio	1sigma	Ratio	1sigma	Ratio	1sigma	rho	Ratio	Age (Ma)	1sigma	Age (Ma)	1sigma	Age (Ma)	1sigma	
Sample RJW1416, rhyolite from the Khamal Formation, Sindreh Basin, N.24°50′01.7″ E.73°47′16.4″																		
RJW1416-01	73	77.7	83.4	0.0714	0.0016	1.2386	0.0333	0.1255	0.0020	0.60	1.12	969	46	818	15	762	12	93.2
RJW1416-02	53.7	58.5	67.3	0.0708	0.0016	1.2033	0.0232	0.1245	0.0022	0.94	1.05	950	44	802	11	756	13	94.3
RJW1416-03	55.0	57.7	52.3	0.0720	0.0021	1.2427	0.0394	0.1248	0.0018	0.46	1.33	987	59	820	18	758	10	92.5
RJW1416-04	95	116	89.3	0.0680	0.0015	1.1697	0.0241	0.1250	0.0017	0.65	1.56	878	44	786	11	759	10	96.5
RJW1416-05	95	114	90.6	0.0658	0.0011	1.1356	0.0211	0.1250	0.0015	0.64	1.52	798	36	770	10	759	9	98.5
RJW1416-06	74	80.0	92.4	0.0705	0.0015	1.2139	0.0268	0.1251	0.0019	0.69	1.05	944	44	807	12	760	11	94.1
RJW1416-07	110	117	151	0.0659	0.0011	1.1388	0.0245	0.1254	0.0022	0.82	0.94	803	35	772	12	762	13	98.7
RJW1416-08	405	450	665	0.0650	0.0007	1.1258	0.0155	0.1255	0.0014	0.83	0.83	772	23	766	7	762	8	99.5
RJW1416-09	185	210	183	0.0646	0.0012	1.1182	0.0235	0.1257	0.0021	0.78	1.42	763	238	762	11	763	12	100.1
RJW1416-10	83	90.1	95.5	0.0703	0.0016	1.2204	0.0277	0.1266	0.0026	0.89	1.14	939	46	810	13	769	15	94.9
RJW1416-11	102	110	134	0.0583	0.0012	1.0195	0.0231	0.1268	0.0019	0.68	0.99	543	46	714	12	770	11	107.8
RJW1416-12	64	73.6	55.5	0.0682	0.0018	1.1947	0.0347	0.1268	0.0022	0.60	1.61	876	56	798	16	770	13	96.5
RJW1416-13	60	63.9	70.2	0.0682	0.0015	1.2514	0.0312	0.1334	0.0024	0.73	1.11	872	46	824	14	807	14	98.0
RJW1416-14	80	81.2	110	0.0734	0.0021	1.3673	0.0511	0.1338	0.0021	0.42	0.90	1033	59	875	22	809	12	92.5
RJW1416-15	78	82.0	68.4	0.0613	0.0016	1.1413	0.0288	0.1355	0.0021	0.60	1.48	650	54	773	14	819	12	106.0
Sample RJW1418, rhyolite from the Angor Formation, Sindreh Basin, N.24°52′49.2″ E.73°46′45.1″																		
RJW1418-01	71	89.7	87.2	0.0648	0.0014	1.1236	0.0272	0.1258	0.0018	0.60	1.26	766	45	765	13	764	10	99.9
RJW1418-02	100	123	104	0.0672	0.0013	1.1644	0.0240	0.1257	0.0015	0.57	1.46	843	158	784	11	763	9	97.4
RJW1418-03	92	117	148	0.0637	0.0011	1.0996	0.0209	0.1253	0.0016	0.65	0.97	731	37	753	10	761	9	101.0
RJW1418-04	116	202	96	0.0755	0.0018	1.2944	0.0330	0.1244	0.0016	0.50	2.14	1081	48	843	15	756	9	89.6
RJW1418-05	55.0	74.7	63.3	0.0672	0.0015	1.1668	0.0296	0.1261	0.0018	0.55	1.45	844	53	785	14	766	10	97.5
RJW1418-06	119	136	185	0.0662	0.0010	1.1687	0.0212	0.1281	0.0014	0.62	0.91	813	27	786	10	777	8	98.8
RJW1418-07	65	77.5	76.4	0.0665	0.0013	1.1753	0.0277	0.1282	0.0018	0.60	1.25	833	38	789	13	777	10	98.5
RJW1418-08	43.4	46.2	42.4	0.0678	0.0021	1.1943	0.0400	0.1282	0.0024	0.55	1.33	863	64	798	19	778	13	97.5
RJW1418-09	147	175	137	0.0650	0.0012	1.1393	0.0226	0.1274	0.0016	0.65	1.59	776	35	772	11	773	9	100.1
RJW1418-10	37.3	44.9	48.9	0.0652	0.0018	1.1246	0.0319	0.1262	0.0025	0.70	1.12	781	58	765	15	766	14	100.1
RJW1418-11	100	109	103	0.0775	0.0015	1.3582	0.0300	0.1275	0.0020	0.72	1.27	1144	38	871	13	773	12	88.8
RJW1418-12	102	119	98	0.0653	0.0012	1.1571	0.0251	0.1285	0.0017	0.60	1.48	785	44	781	12	780	10	99.9
RJW1418-13	96	107	140	0.0648	0.0011	1.1428	0.0222	0.1279	0.0016	0.66	0.94	769	37	774	11	776	9	100.3
RJW1418-14	117	232	110	0.0786	0.0017	1.3351	0.0267	0.1243	0.0021	0.85	2.13	1161	43	861	12	755	12	87.7
RJW1418-15	59.1	70.9	61.4	0.0697	0.0021	1.2030	0.0321	0.1274	0.0029	0.87	1.38	918	68	802	15	773	17	96.4

[a] Degree of concordance = 100*($^{206}Pb/^{238}U$ age/$^{207}Pb/^{235}U$ age).

Table 2
Sr-Nd isotopes for the volcanic rocks from the Sindreth and Punagarh basins and the Malani Igneous Suites.

Sample	Lithology	U–Pb age	Rb (ppm)	Sr (ppm)	$^{87}Rb/^{86}Sr$	$^{87}Sr/^{86}Sr$	$\pm2\sigma$	$^{87}Sr/^{86}Sri$	Sm (ppm)	Nd (ppm)	$^{147}Sm/^{144}Nd$	$^{143}Nd/^{144}Nd$	$\pm2\sigma$	$\varepsilon_{Nd(t)}$	T_{DM} (Ma)	T^1_{DM2} (Ma)	$f_{Sm/Nd}$	Note
Sindreth group																		
RJW14–11	Rhyolite	760	269	72.4	10.86	0.816457	17	0.698647	18.6	96.1	0.1170	0.512093	7	−2.89	1661	1672	−0.41	This study
RJW14–12	Rhyolite	760	265	56.5	13.73	0.841815	17	0.692787	21.0	107	0.1187	0.512074	6	−3.43	1722	1715	−0.40	This study
RJW14–15	Rhyolite	760	254	73.0	10.19	0.815107	11	0.704496	15.6	81.5	0.1155	0.512239	8	0.11	1412	1429	−0.41	This study
RJW14–17	Rhyolite	760	325	63.1	15.11	0.857724	15	0.693771	22.6	114	0.1201	0.512181	7	−1.47	1575	1557	−0.39	This study
RJW14–18	Rhyolite	760	206	69.9	8.60	0.796112	16	0.702793	13.8	71.2	0.1171	0.512123	6	−2.31	1617	1625	−0.40	This study
BVL-0057	Rhyolite	760							11.7	35.6	0.1994	0.512554	4	−1.90	6243	1575	0.01	Van Lente et al., 2009
RJW14–21	Basalt	760	4.40	596	0.021	0.705820	17	0.705588	10.0	41.3	0.1463	0.512461	5	1.45	1556	1320	−0.26	This study
RJW14–23	Basalt	760	73.6	234	0.909	0.715379	14	0.705515	8.7	38.7	0.1366	0.512421	7	1.61	1440	1307	−0.31	This study
RJW14–24	Basalt	760	88.2	102	2.505	0.733608	10	0.706424	12.8	59.1	0.1309	0.512326	5	0.31	1514	1413	−0.33	This study
RJW14–25	Basalt	760	1.10	59.5	0.054	0.707997	11	0.707416	8.6	37.9	0.1371	0.512275	4	−1.29	1737	1542	−0.30	This study
BVL-0037A	Basalt	760							24.0	106	0.1364	0.512431	3	1.83	1416	1290	−0.31	Van Lente et al., 2009
BVL-0038	Basalt	760							4.9	21.3	0.1386	0.512529	4	3.53	1259	1152	−0.30	Van Lente et al., 2009
BVL-0046C	Basalt	760							8.8	38.8	0.1366	0.512377	3	0.75	1525	1377	−0.31	Van Lente et al., 2009
BVL-0047A	Dolerite	760							7.8	35.3	0.1331	0.512450	3	2.52	1322	1233	−0.32	Van Lente et al., 2009
BVL-0049	Basalt	760							13.0	51.0	0.1539	0.512316	4	−2.12	2117	1608	−0.22	Van Lente et al., 2009
Punagarh group																		
RJW14–56	Dacite	760	235	298	2.285	0.74193	15	0.717134	13.4	58.5	0.1384	0.511866	7	−9.41	2585	2196	−0.30	This study
RJW14–58	Dacite	760	100	154	1.882	0.738381	12	0.717961	10.0	46.5	0.1293	0.511891	7	−8.04	2264	2087	−0.34	This study
RJW14–59	Dacite	760	62.9	351	0.520	0.721384	11	0.715745	11.2	52.8	0.1285	0.511906	5	−7.66	2215	2056	−0.35	This study
RJW14–62	Dacite	760	110	190	1.671	0.735505	11	0.717371	9.9	46.2	0.1297	0.511921	6	−7.49	2221	2042	−0.34	This study
BVL–005B	Dacite	760							8.0	36.7	0.1312	0.512358	4	0.91	1461	1364	−0.33	Van Lente et al., 2009
BVL–0016(2)	Dolerite	760							3.8	13.1	0.1753	0.512793	4	5.11	1415	1023	−0.11	Van Lente et al., 2009
BVL–0019(2)	Basalt	760							5.3	18.6	0.1736	0.512759	3	4.61	1484	1063	−0.12	Van Lente et al., 2009
BVL–0020	Dolerite	760							6.0	21.2	0.1710	0.512774	4	5.16	1339	1018	−0.13	Van Lente et al., 2009
BVL–005C	Basalt	760							5.6	18.6	0.1816	0.512653	6	1.77	2346	1292	−0.08	Van Lente et al., 2009
BVL-005C(2)	Basalt	760							5.4	17.7	0.1825	0.512651	4	1.64	2423	1302	−0.07	Van Lente et al., 2009
BVL–008B	Basalt	760							5.8	19.7	0.1780	0.512686	23	2.76	1973	1212	−0.10	Van Lente et al., 2009
BVL–008B(2)	Basalt	760							5.6	19.1	0.1781	0.512626	4	1.58	2234	1308	−0.09	Van Lente et al., 2009
Malni Igneous Suites																		
RJW14–82	Rhyolite	760	157	21.7	21.32	0.879082	10	0.647720	21.1	91.1	0.1400	0.512698	14	6.70	935	894	−0.29	This study
RJW14–83	Rhyolite	760	205	17.8	34.14	0.975822	12	0.605384	16.8	78.2	0.1299	0.512608	7	5.92	986	958	−0.34	This study
RJW14–97	Rhyolite	760	139	28.3	14.41	0.836995	12	0.680640	4.8	13.7	0.2146	0.512989	13	5.11	−29,370	1082	0.09	This study
RJW14–84	Rhyolite	760	137	58.5	6.820	0.769550	14	0.695553	13.0	55.4	0.1420	0.512734	5	7.20	885	854	−0.28	This study

1: $T_{DM2} = T_{DM} - (T_{DM}\text{-rock age}) * (-0.4 - (^{147}Sm/^{144}Nd/0.1967 - 1))/(-0.4 - 0.08592)$

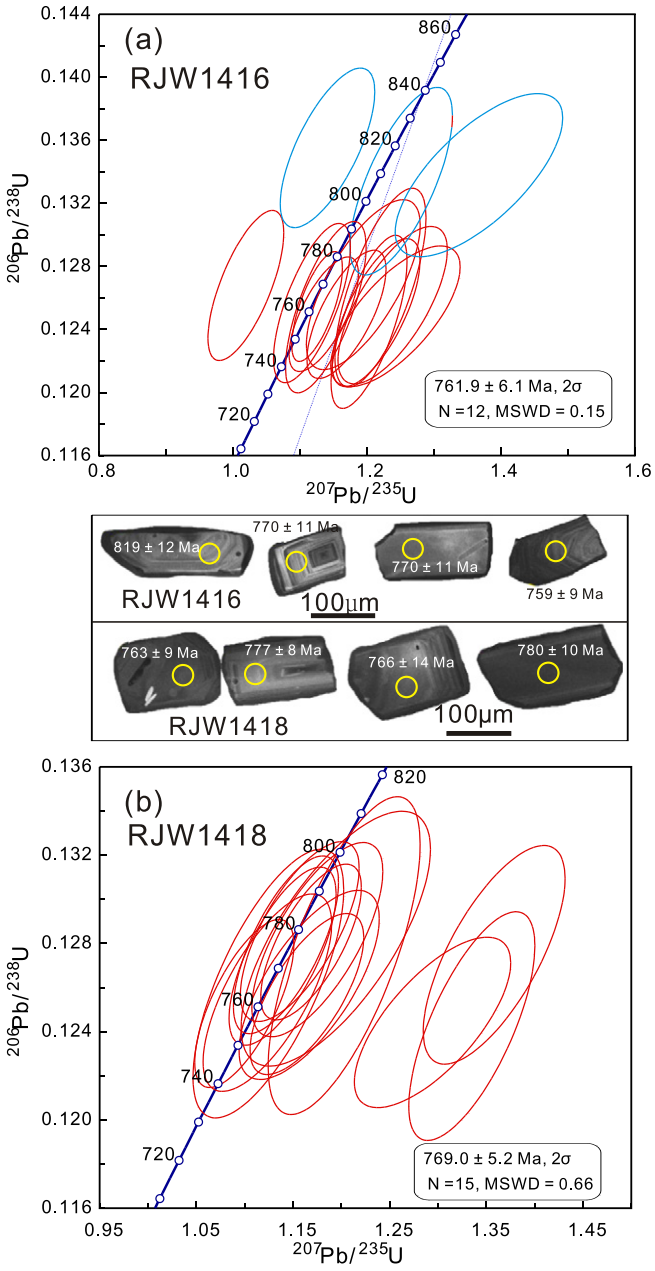

Fig. 4. Concordia diagrams for the U-Pb isotopes of zircons from the Sindreth rhyolites. Morphology and internal structures of typical zircons are also shown. Blue circles represent the data for inherited zircons that are not included in age calculations. The marked ages in the CL images refer to $^{206}Pb/^{238}U$ ages.

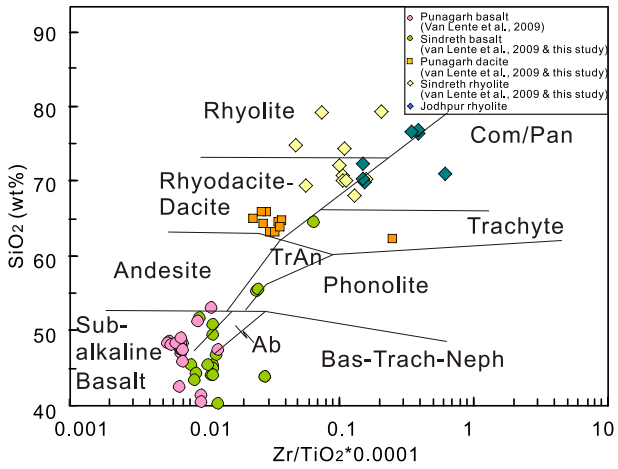

Fig. 5. Rock classification diagram Nb/Y versus $Zr/TiO_2 \times 0.0001$ showing the bimodal nature of volcanic rocks in NW India (modified after Winchester and Floyd, 1976). Data for some the Punagarh basalt and dacite as well as the Sindreth basalt and rhyolite are compiled from Van Lente et al. (2009). Details of data compilations are provided in Table S2.

10.1 wt%), P_2O_5 (1.96–0.20 wt%), MgO (5.77–1.16 wt%) and CaO (9.07–1.69 wt%) (Table S2). Relatively high TiO_2 content of Sindreth basalts indicates alkaline affinity while Punagarh basalts are largely sub-alkaline (Fig. 5). Most samples lack linear trends and systematic correlations in the Harker diagrams except a moderately negative correlation between SiO_2 and $Fe_2O_3^T$ (Fig. 6). Besides, Al_2O_3 shows slight negative correlation with MgO, whereas TiO_2 and CaO lack any linear correlation with MgO.

Although the Sindreth basalts have trace elemental concentrations generally higher than the Punagarh basalts, both show similar primitive mantle normalized trace-element patterns that are characterized by enrichment of large ion lithophile trace elements (LILE) and depletion of high field strength elements (HFSE) (Figs. 7a and b). Negative Nb, Ta and P anomalies are observed in all the samples and three Sindreth basalt samples also show prominent negative Ti anomalies (Fig. 7a). In the chondrite normalized Rare Earth Element (REE) diagrams the Sindreth basalts show OIB-like patterns, except slight to moderate negative Eu anomalies (Fig. 8a) whereas most Punagarh basalts show N-MORB signatures (Fig. 8b).

4.2.2. Rhyolites and dacites

The felsic volcanic rocks show high and variable SiO_2 content (79.3–63.2 wt%). Rhyolites from the Sindreth Basin and Jodhpur region show similar high and variable $K_2O + Na_2O$ (9.91–1.65 wt%) and low CaO (0.90–0.09 wt%) contents (Table S2). The Punagarh dacites have lower SiO_2 (65.8–62.2 wt%) and $K_2O + Na_2O$ (7.71–2.78 wt%) contents and higher $Fe_2O_3^T$ (8.66–5.69 wt%) and CaO (4.39–0.56 wt%) abundance as compared to the studied rhyolites.

The rhyolite trace element patterns show prominent negative anomalies for Nb, Ta, P and Ti (Fig. 7c). The Jodhpur rhyolites have relatively high HFSE contents and show significantly positive Zr-Hf anomalies, in contrast to the negative Zr-Hf anomalies observed in Sindreth rhyolites (Fig. 7c). In addition, the Jodhpur rhyolite samples have less fractionated REE patterns [$(La/Yb)_{CN} = 4.08–(0.67)$] and more prominent Eu anomalies ($Eu/Eu^* = 0.51–0.12$), relative to Sindreth rhyolites [$(La/Yb)_{CN} = 11.5–1.75$ and $Eu/Eu^* = 0.73–0.20$] (Fig. 8c). The Punagarh dacites show significant depletion of Nb, Ta, P and Ti, and slightly negative Zr-Hf anomalies, except one sample showing Zr and Hf enrichment (Fig. 7d). The dacites have moderately fractionated REE patterns with [$(La/Yb)_{CN} = 7.69–5.51$] and smaller negative Eu anomalies ($Eu/Eu^* = 0.75–0.38$), relative to rhyolites (Fig. 8d).

4.3. Bulk rock Sr-Nd isotopes

The Sindreth basalts have slightly variable $^{147}Sm/^{144}Nd$ (0.1539–0.1309) and $^{144}Nd/^{143}Nd$ (0.512461–0.512275) ratios (Table 2) and $\varepsilon_{Nd(t)}$ values ranging from +3.5 to −2.1. They also show variable $^{87}Rb/^{86}Sr$ ratios (2.505 to 0.021) and initial $^{87}Sr/^{86}Sr$ ratios (0.707416 to 0.705515). In contrast, the Punagarh basalts have higher $^{147}Sm/^{144}Nd$ (0.1825–0.1710) and $^{144}Nd/^{143}Nd$ (0.512793–0.512626) ratios, corresponding to radiogenic $\varepsilon_{Nd(t)}$ values ranging from +5.11 to +1.58, (Table 2) (van Lente et al., 2009).

Each group of the felsic volcanic rocks has distinct Nd isotopic compositions (Table 2). The Jodhpur rhyolites have high $\varepsilon_{Nd(t)}$ values (+7.2 to +5.1) and young T_{DM2} ages (1082–854 Ma), while Punagarh dacites show remarkably negative $\varepsilon_{Nd(t)}$ values (−7.5 to −9.4) and old T_{DM2}

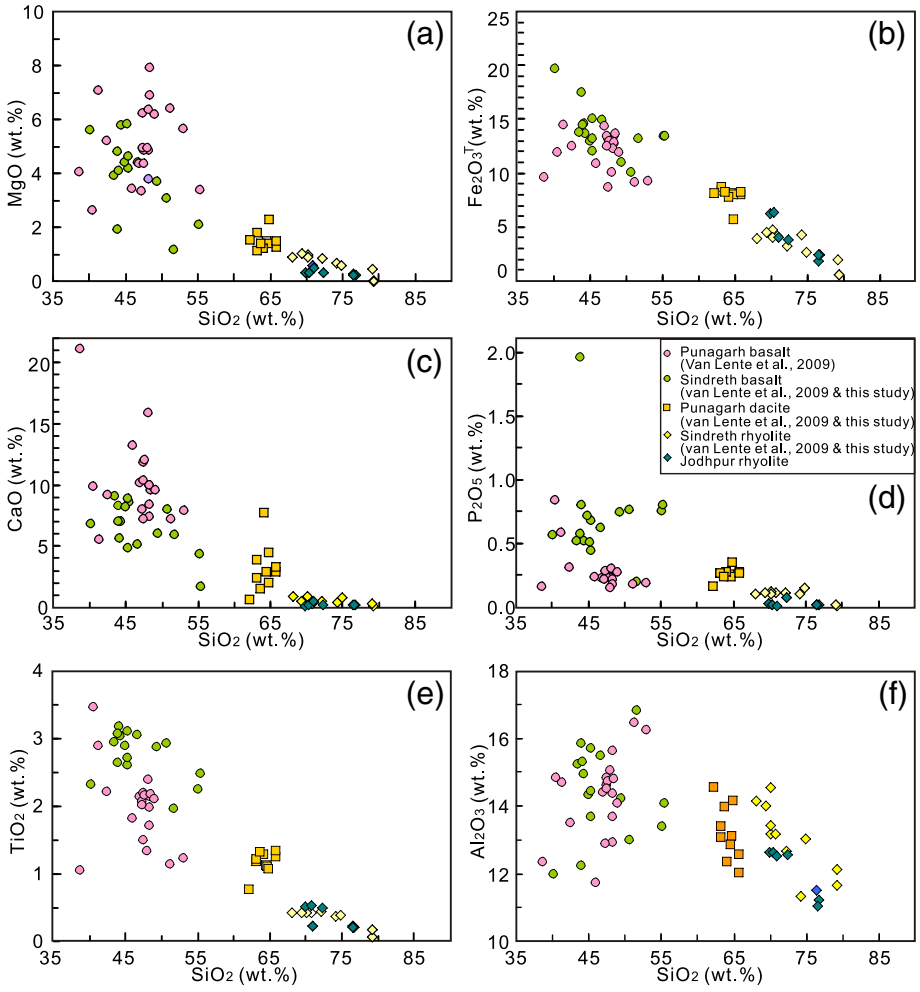

Fig. 6. The SiO_2 variation diagrams versus MgO, CaO, P_2O_5 and $Fe_2O_3^T$, and MgO versus $Fe_2O_3^t$, Al_2O_2, CaO and TiO_2 plots for bimodal volcanic rocks from NW India.

ages (2196–2042 Ma). The Sindreth rhyolites have near zero to moderately negative $\varepsilon_{Nd(t)}$ values (+0.1 to −3.4) and 1715–1429 Ma T_{DM2} ages. Both Sindreth and Jodhpur rhyolites show unrealistically low initial $^{87}Sr/^{86}Sr$ ratios (0.702793–0.605384) that probably resulted from disturbance of the Rb-Sr isotopic systems, while the Punagarh dacites have high initial $^{87}Sr/^{86}Sr$ ratios (0.717961–0.715371), possibly inherited from an old crustal source material.

5. Discussion

5.1. Effect of hydrothermal alteration

The Sindreth and Punagarh basalts are hydrothermally altered but have still preserved igneous textures, such as subrounded amygdales and vesicles and elongate and randomly oriented microphenocrysts of plagioclase (van Lente et al., 2009). Their alkali element and LILE distribution patterns testify the effect of alteration, as indicated by their variable concentrations and lack of systematic fractionation trends. The REE, HFSE, Cr and Ni are considered as immobile as they remain unaffected during alteration (Arndt, 1994; Jochum et al., 1991), however, they may become mobile during intense carbonic hydrothermal alteration and/or metamorphism (Lahaye and Arndt, 1996). The Zr is considered as one of the least mobile elements and thus has been successfully employed for petrogenetic interpretations for altered and low to moderate grade metamorphosed rocks (Pearce and Peate, 1995; Polat et al., 2002; Winchester and Floyd, 1976). In the present case, the mobile elements like Rb and Sr display non-linear correlations with Zr (Figs. 9a and b), while Th, Ti, Nb and REE show well correlated relationships with Zr, indicating their immobility. In addition, HFSE and some transition elements also show similar patterns in the primitive mantle-normalized diagrams (Fig. 7). The Sindreth and Punagarh basalts demonstrate coherent REE patterns and negligible Ce anomalies, consistent with their immobility during alteration (Fig. 8). Therefore the mobile elements were screened out from further discussion and petrogenetic interpretations.

5.2. Magma differentiation and crustal contamination of basaltic rocks

Fractional crystallization and crustal contamination play important role in the petrogenesis of the basaltic rocks, reflected in modifications in elemental and isotopic compositions (DePaolo, 1981). The Sindreth and Punagarh basalts do not show clear correlations between $Fe_2O_3^T$ and MgO, precluding a prominent olivine (forsterite) fractionation. Therefore, the negative correlation between MgO and SiO_2 in the Punagarh basalt may be attributed to clinopyroxene fractionation, which is also evidenced by a positive correlation between Al_2O_3 and MgO (Fig. 6f). The Sindreth basalts show negative correlation between SiO_2 and CaO, further corroborating clinopyroxene and plagioclase fractionation. The plagioclase crystallization is also indicated by moderate negative Eu anomalies (Fig. 8a). Insignificant positive correlation between MgO and CaO in Sindreth samples can therefore be attributed to simultaneous crystallization of clinopyroxene and plagioclase. In great contrast, Punagarh basalts fail to show any correlative relationship

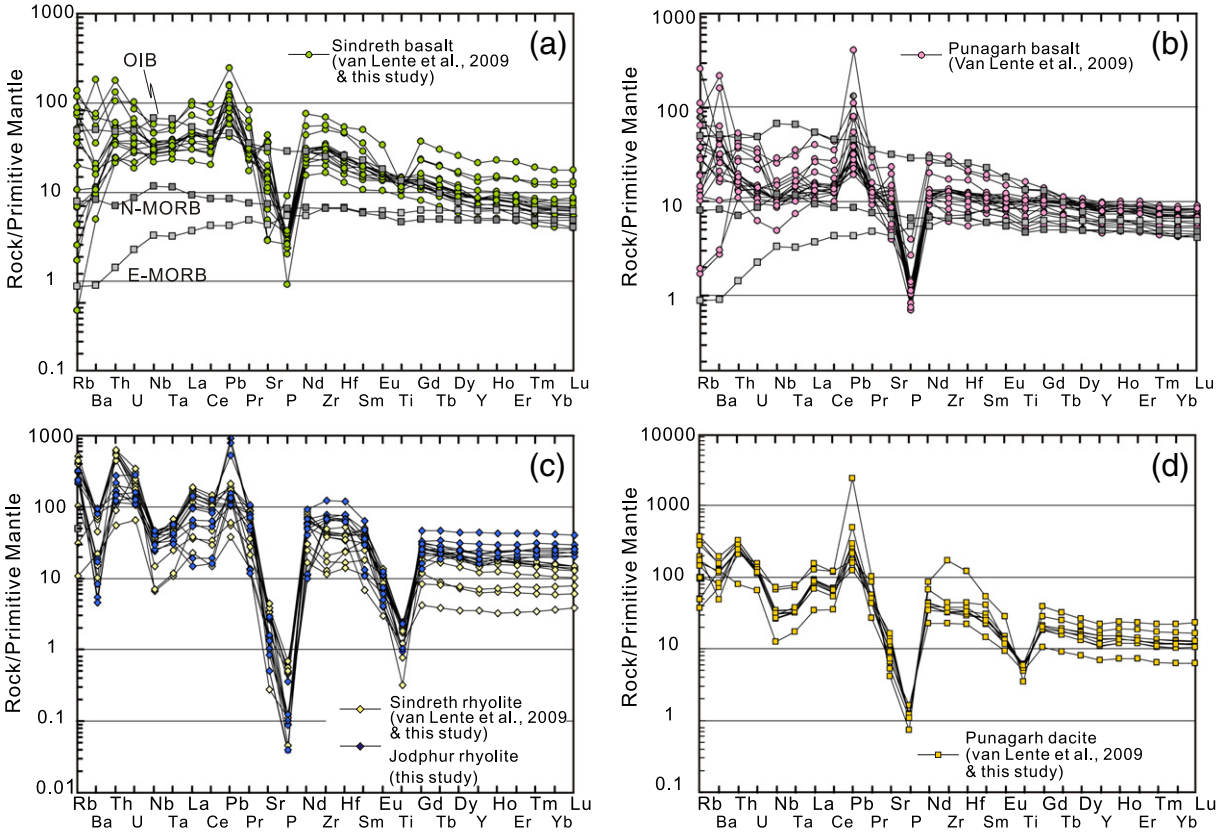

Fig. 7. Primitive mantle-normalized trace element patterns for the bimodal volcanic rocks of NW India. Normalization values after Sun and McDonough (1989).

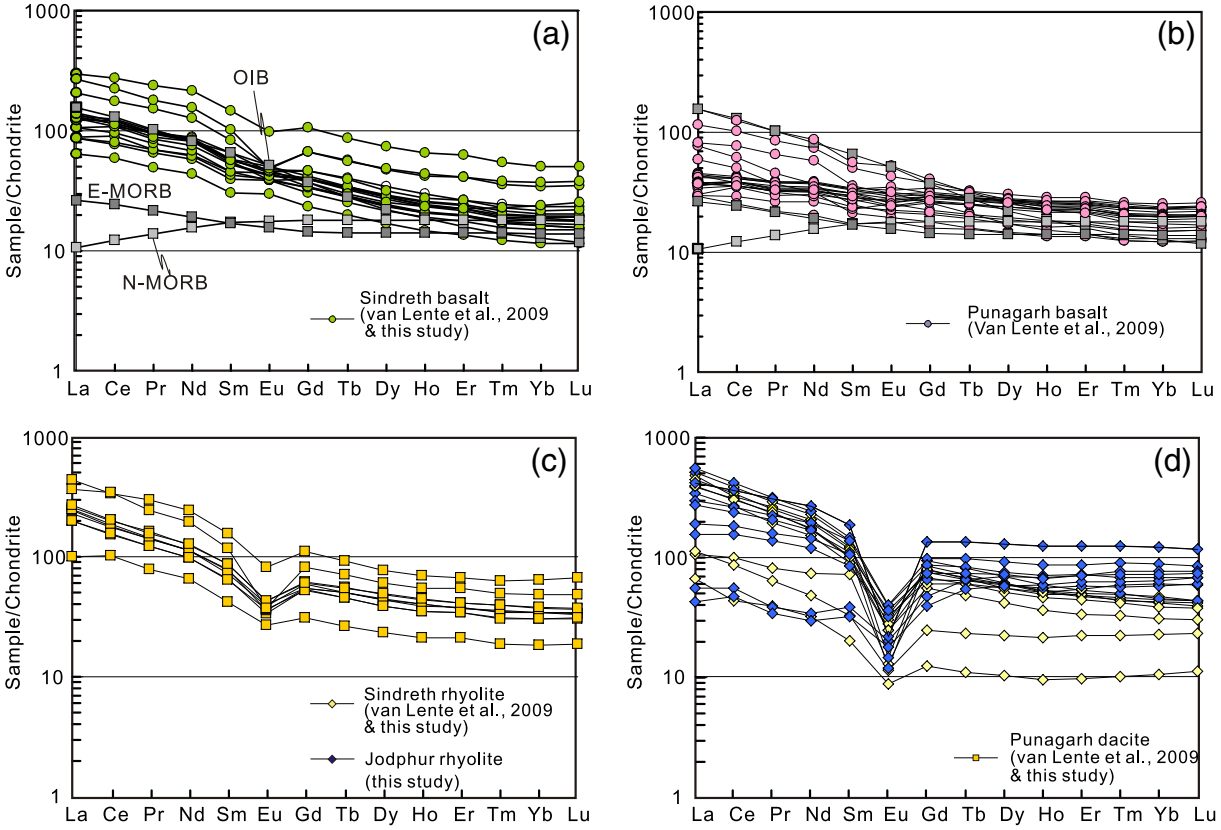

Fig. 8. Chondrite-normalized REE patterns of the bimodal volcanic rocks of NW India. Normalization values after Sun and McDonough (1989).

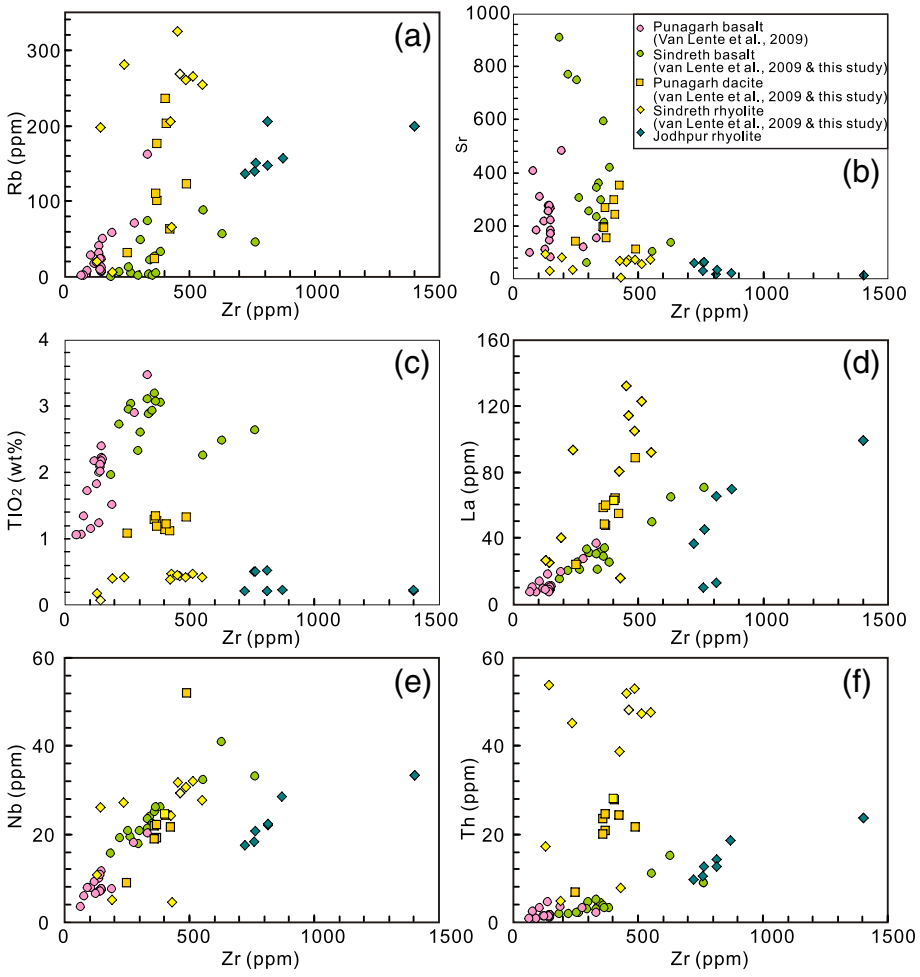

Fig. 9. Bi-elemental plots of Zr versus TiO_2, Rb, Sr, La, Nb and Th to evaluate the mobility of these elements in studied bimodal volcanic rocks during metamorphism and hydrothermal alteration.

among SiO_2-MgO, SiO_2-CaO and MgO-TiO_2 pairs, indicative of insignificant influence of fractionation on magma evolution.

The Sindreth and Punagarh basalts show positive Pb and negative Nb-Ta anomalies in the multi-element spider diagrams that probably resulted from crustal contamination (Figs. 7b). Nonetheless, minor crustal contamination would also produce Zr and Hf enrichment and Ti depletion (Rudnick and Gao, 2003), not observed in the Punagarh basalts (Figs. 7b). The Sindreth basalts show Ti depletion, however, slight negative Zr-Hf anomalies rule out any significant crustal contamination. All the basalt samples have low Th/Nb (average = 0.21) and La/Nb ratios (average = 1.37), both within the ranges considered for pristine basalts unaffected by substantial crustal influence (Condie, 2003; Kerrich et al., 1999). In addition, $\varepsilon_{Nd(t)}$ values for all the basalt samples lack any systematic correlation with SiO_2 (Fig. 10a), further suggesting insignificant crustal contamination during magma evolution. Therefore, variations in elemental and Nd isotopic signatures in Sindreth and Punagarh basalts indicate heterogeneous magma sources for them.

5.3. Heterogeneous mantle sources for Sindreth and Punagarh basalts

As discussed in preceding section, hydrothermal alteration and crustal assimilation can be ruled out as possible causes for distinctive geochemical characteristics of Sindreth and Punagarh basalts. Their specific compositional features are probably inherited from their mantle sources. The Punagarh and Sindreth basalts show different trends in Harker diagrams, in particular, in SiO_2-P_2O_5, SiO_2-MgO and SiO_2-CaO plots (Fig. 6), suggestive of chemically distinct mantle sources. Their dissimilar Nb/Y and La/Yb ratios further underline chemically diverse mantle source as these elements have similar geochemical behavior during partial melting and magma fractionation. Higher $\varepsilon_{Nd(t)}$ values (+5.2 to +1.6) in Punagarh basalts as compared to Sindreth basalts (+3.5 to −2.1), in combination with variable LREE enrichment and HFSE (Nb, Ta and Ti) depletion, provide definitive evidence to infer isotopically and geochemically distinct mantle source compositions for Punagarh and Sindreth basalts.

5.3.1. Shallow mixed asthenospheric-lithospheric mantle source for Punagarh basalts

The Punagarh basalts define slightly LREE-enriched and flat HREE patterns and minor (slightly negative to positive) Eu anomalies, similar to typical E-MORB (Figs. 7 and 8). Most of the Punagarh basalt samples have La/Yb (6.23–2.19) and Ti/V (40.9–28.2) ratios comparable to MORB but distinct from OIB (Fig. 11a). They plot within the MORB field in the Ti-Zr diagram (Fig. 11b) and have relatively more radiogenic Nd isotopic compositions ($\varepsilon_{Nd(t)}$ = +5.2 to +1.6), in agreement with a depleted mantle source. A positive correlation between $\varepsilon_{Nd(t)}$ and Nb/La (Fig. 10b), however, reveals mixing of two isotopically distinct components because crustal assimilation has been ruled out. The depleted component can be interpreted as the asthenospheric mantle, as suggested above, while the enriched component may be the lithospheric mantle since continental crustal signatures, such as depletion of Zr, Hf and Ti, are absent. The geochemical and isotopic signatures can be interpreted in terms of a mixed mantle source involving asthenospheric

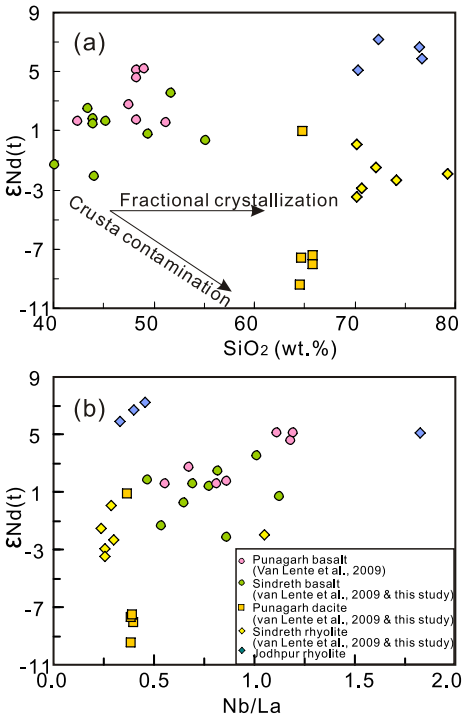

Fig. 10. The $\varepsilon_{Nd(t)}$ values versus SiO_2 and Nb/La ratios diagrams showing insignificant influence of crustal contamination in Sindreth and Punagarh volcanics during magma evolution.

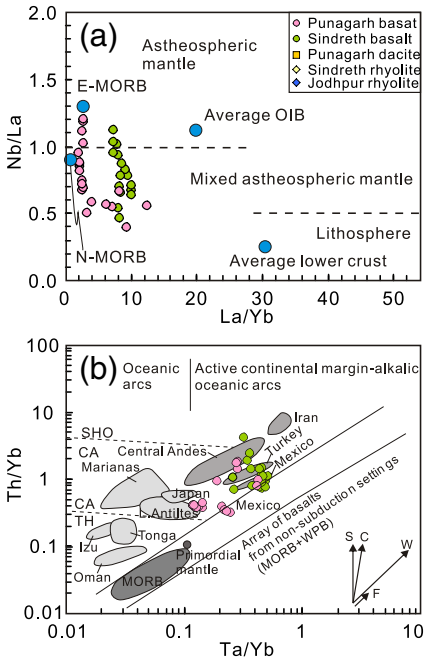

Fig. 12. Elemental ratio plots for the bimodal Sindreth and Punagarh volcanic rocks; (a) La/Nb versus Ba/Nb with data sources: PM primitive mantle (Sun and McDonough, 1989); Average lower continental crust (Condie, 1993; Taylor and McLennan, 1985); OIB (Le Roex, 1986); (b) Th/Yb versus Ta/Yb (Pearce, 1983). Abbreviation: S - subduction zone enrichment; C - crustal contamination; W – within plate enrichment; F - fractional crystallization.

and lithospheric components, also revealed by the variable Nb/La ratios (Fig. 12a).

The Punagarh basalts have low Sm/Yb and La/Sm ratios, consistent with a spinel-bearing mantle source, which has undergone 10–20% partial melting to generate the primary basaltic magma (Fig. 13). This implies that the decompression induced asthenospheric mantle ascent to a relatively shallow level, i.e. <85 km, where the transition from garnet to spinel in the mantle occurs (Robinson and Wood, 1998).

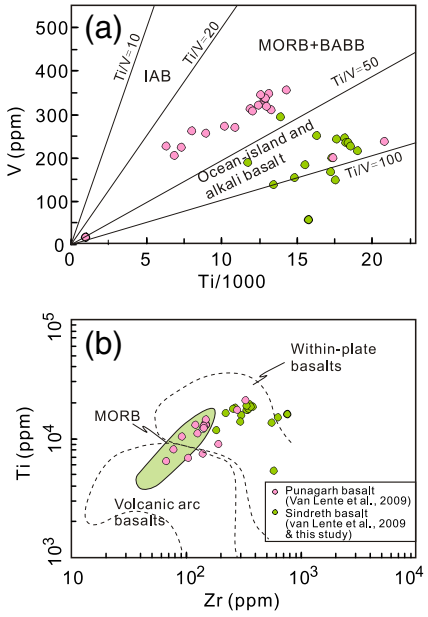

Fig. 11. Elemental concentration and elemental ratio plots for the Sindreth and Punagarh bimodal volcanic rocks; (a) Ti versus V (after Shervais, 1982); (b) Ti versus Zr (after Meschede, 1986).

5.3.2. Slab melt enriched asthenospheric mantle source for Sindreth basalts

Although the Sindreth basalts display a prominent Nb-Ta trough, a characteristic of arc-related magma systems (Fig. 7), they have TiO_2 (3.18–1.96 wt%) and Nb (10.9–15.5 ppm) contents higher than typical intra-oceanic arc basalts (TiO_2 < 1 wt% and Nb <2 ppm). The Sindreth basalts show pronounced LREE fractionated patterns with high $(La/Yb)_{CN}$ ratios of 7.24–5.24, hinting at the stability of garnet in the mantle source. This inference is further supported by their Sm/Yb and La/Sm ratios that are higher than the spinel-lherzolite melting curve but lower than the garnet-lherzolite melting trend (Fig. 13a), indicating a spinel-garnet lherzolite mantle source (Aldanmaz et al., 2000; Siddiqui and Ma, 2017). Relatively low degree (~5%) of partial melting probably resulted in high abundance of incompatible elements in the Sindreth basalts. These basalts have high TiO_2 (3.18–1.96 wt%), high Zr (762–183 ppm) and high Ti/V ratios (285–47.6), consistent with ocean-island and alkali basalt affinity (Figs. 11a and b). Therefore, the Sindreth basalts were derived from a deeper asthenospheric source as compared to the shallow mantle derived Punagarh basalts.

Depletion of Nb-Ta and Ti in the Sindreth basalts can be attributed to enrichment of the mantle source as crustal contamination has been precluded in the preceding sections. The enriched components, therefore, were most likely sourced from the oceanic sediments, as constrained by their relatively non-radiogenic Nd isotopic compositions ($\varepsilon_{Nd(t)}$ = +3.5 to −2.1). Oceanic sediment derived melts are believed to be the candidates to interact with asthenospheric mantle as evidenced by the low Ba/Y and Th/Zr ratios, suggesting a slab melt enriched mantle source for Sindreth basalts (Fig. 14).

5.4. Petrogenesis of the felsic volcanic rocks

Coexisitng felsic volcanic rocks (rhyolite and dacite) in Sindreth and Punagarh basins and adjacent Jodhpur area have variable SiO_2 (79.3–62.2 wt%), high alkali contents (9.90–2.78 wt%), moderate to low CaO

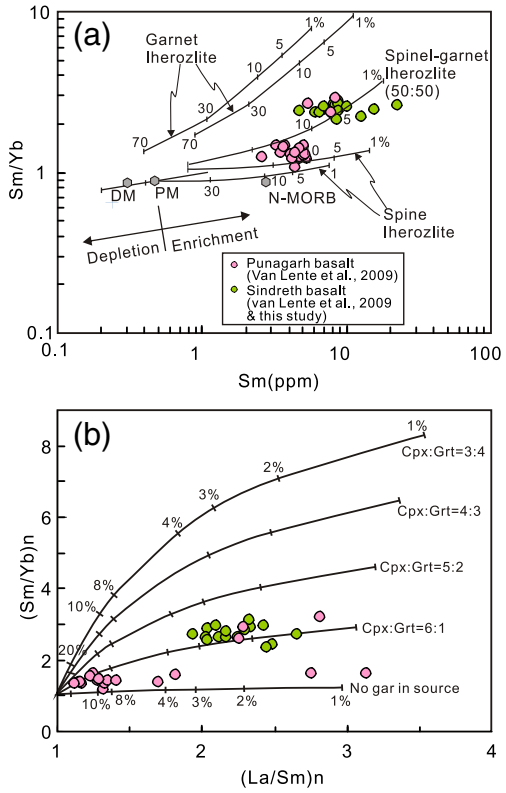

Fig. 13. (a) Sm/Yb vs. Sm plot for the Sindreth and Punagarh bimodal volcanic rocks. Mantle array (heavy line) defined by depleted MORB mantle (DMM, McKenzie and O'Nions, 1991) and primitive mantle (PM, Sun and McDonough, 1989). Melting curves for spinel lherzolite (Ol53 + Opx27 + Cpx17 + Sp11) and garnet peridotite (Ol60 + Opx20 + Cpx10 + Gt10) with both DMM and PM compositions are after Aldanmaz et al. (2000). Numbers along lines represent the degree of the partial melting; (b) Sm/Yb versus La/Sm diagram. Batch melting trends for various clinopyroxene/garnet ratios in the residue solid are taken from D'Orazio et al. (2001).

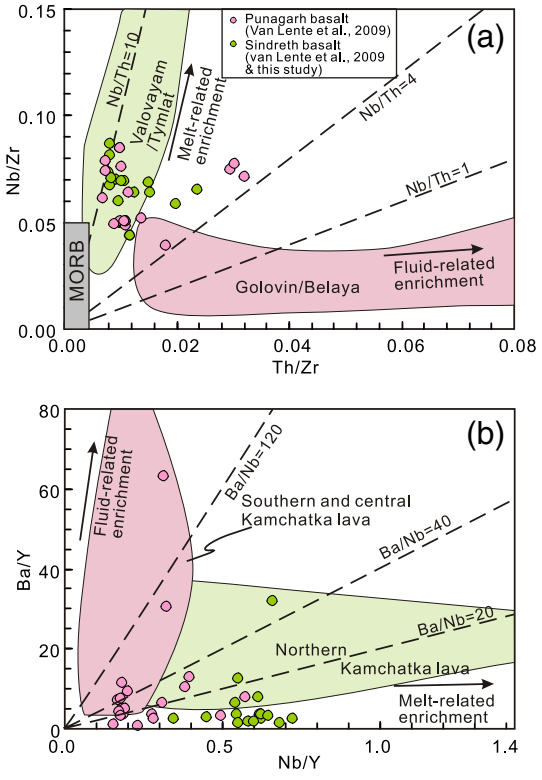

Fig. 14. Plots of Th/Zr vs. Nb/Zr (a) and Nb/Y vs. Ba/Y (b) for the bimodal volcanic rocks at NW India. Fields for the Kamchatka, Golovin/Belaya and Valovayam/Tymlat lavas are from Kepezhinskas et al. (1997).

(7.66–0.09 wt%) and MgO contents (1.76–0.22 wt%). They show high Ga/Al*1000 ratios (4.9–2.2) and high HFSE concentrations as well as significant negative Eu and Sr anomalies (Table S2) (Fig. 6), similar to those described for A-type granites (Collins et al., 1982; Loiselle and Wones, 1979; Whalen et al., 1987). Additionally, all the samples plot in the field of A-type granites in the 1000*Ga/Al vs. (Zr + Nb + Ce + Y) diagram (Fig. 15a). The zircon saturation temperatures have been estimated between 1062 and 779 °C (average = 864 °C) for Sindreth rhyolites and Punagarh dacite, and between 1000 and 949 °C for Jodhpur rhyolite, consistent with high temperature A-type magmatism (Clemens et al., 1986).

Proposed petrogenetic models for A-type granites include fractionational crystallization of alkaline basaltic magma (Loiselle and Wones, 1979; Turner et al., 1992) or anatexis of lower crustal granulite, tonalitic I-type or charnockitic rocks (Collins et al., 1982; Jiang et al., 2005; Landenberger and Collins, 1996; Whalen et al., 1987; Zhao et al., 2008). Compared with the associated basalts, the Sindreth rhyolitic and Punagarh dacitic samples have lower $\varepsilon_{Nd(t)}$ values that are non-correlative with SiO_2 (Fig. 10), ruling out the possibility that the felsic rocks are differentiation products of the basaltic melts. Although the Jodhpur rhyolites have high $\varepsilon_{Nd(t)}$ values (+7.2 to +5.1), their low zircon $\delta^{18}O$ values (+4.12‰ to −1.1 ‰) indicate derivation from bulk cannibalization of a hydrothermally altered juvenile crust (Wang et al., 2017b). Moreover, the limited volume of basaltic rocks in the MIS system as well as extreme enrichment of Zr, Nb and Ce, also argue against fractionation of alkaline basaltic magma as the possible mechanism for generation of A-type volcanic rocks in the MIS. Therefore, the studied A-type volcanic rocks were produced by partial melting of heterogeneous mix of crustal rocks as indicated by their variable Nd isotopes. The Jodhpur rhyolites have high $\varepsilon_{Nd(t)}$ values (+7.2 to +5.1) and were probably derived from the juvenile crust whereas the Sindreth rhyolites with relatively low $\varepsilon_{Nd(t)}$ values (+0.1 to −3.4) reflect involvement of more mature crustal materials. The Punagarh dacites, however, have high initial $^{87}Sr/^{86}Sr$ ratios (0.717961 to 0.715745), strong negative $\varepsilon_{Nd(t)}$ values (−9.4 to −7.5) and old T_{DM2} ages (2196 to 2042 Ma), similar to the Paleoproterozoic (~1.66 Ga) granitoids in the Aravalli belt (Kaur et al., 2007), indicating a much older source. Therefore, the felsic volcanics in the study area were derived from partial melting of variable crustal components, likely triggered by upwelling of coeval basaltic magma.

Although the A-type igneous rocks are widely associated with anorogenic or within plate rift environment (Collins et al., 1982; Eby, 1990), granites generated at convergent margin settings can also posses A-type signatures (Eby, 1992; Li et al., 2016; Whalen et al., 1987; Zhang et al., 2017; Zhao et al., 2008). The Jodhpur rhyolites have high Y/Nb (5.97–4.28) and Yb/Ta (9.36–6.99) ratios, resembling A-type magmatic rocks derived from sources chemically similar to those of island arc or continental margin basalts (Eby, 1990, 1992) (Fig. 15b). The Sindreth rhyolites and Punagarh dacites have relatively lower Y/Nb (5.62–1.55) and Yb/Ta (6.28–2.57) ratios, suggesting a *syn*-collision setting (Fig. 15b). In the geochemical discrimination plot of Eby (1992), all the rhyolitic and dacitic samples plot in the A_2 field (Fig. 15c), indicating a continental crustal source that has been through a cycle of continent-continent collision or island-arc magmatism.

5.5. Mantle source heterogeneity and bimodal volcanism: consequence of slab break-off

The spinel-bearing mantle source for the Punagarh basalts requires upwelling of the convective asthenosphere to a relatively shallow level, i.e. <85 km, the depth of transition from spinel to garnet at the peridotite solidus (Robinson and Wood, 1998). This shallow asthenospheric source is inconsistent with the thickness of lithosphere beneath

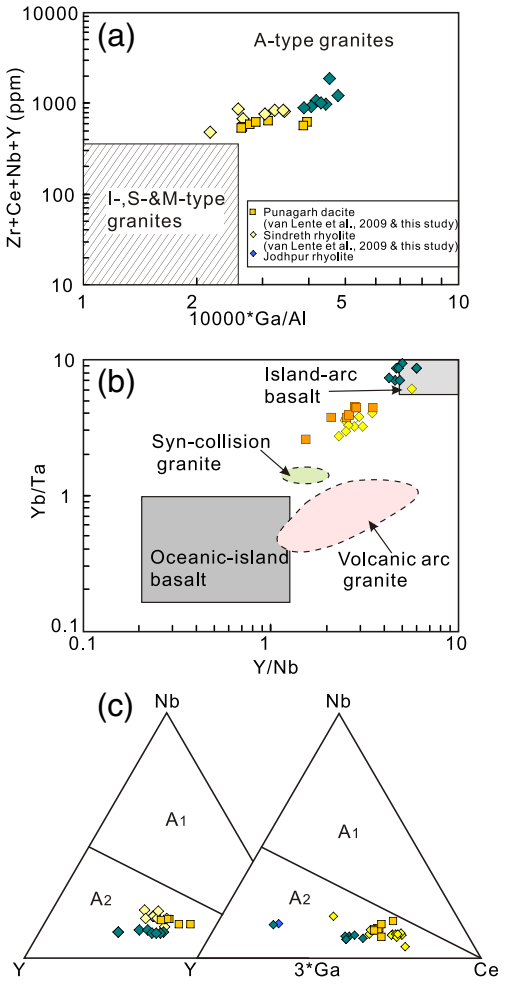

Fig. 15. Plots of the Sindreth and Punagarh bimodal volcanic rocks (a) Zr + Ce + Nb + Y vs.10,000 × Ga/Al diagram (after Whalen et al., 1987) showing an A-type granite affinity; (b) Yb/Ta vs. Y/Nb diagram (Eby, 1992) for Sindreth and Punagarh volcanics exhibiting similarities with IAB; (c) Nb–Y–Nb–Y–Ga and Nb–Y–Ce ternary diagrams (Eby, 1992) showing A_2-subtype granite affinity for Sindreth and Punagarh felsic volcanics.

an overall Andean type accretionary system below the NW Indian continental crust (Ashwal et al., 2013; Collins et al., 2014; T. Torsvik et al., 2001; Wang et al., 2017b). Therefore, it seems quite likely that the lithosphere was locally thinned to allow decompression melting of asthenosphere. Generally, three competing mechanisms, including gravity induced delamination of orogenic root (Gardien et al., 1997), convective thinning of the lithospheric root (Houseman et al., 1981) and slab break-off (von Blanckenburg and Davies, 1995) have been proposed to explain asthenospheric thinning in the orogenic context. Gravity-induced collapse of the orogenic root would produce widespread and intensive asthenosphere-derived mafic magmas (Gardien et al., 1997; Xu et al., 2008), which is not observed in the NW India. A Neoproterozoic OIB-like magmatism is limited to the Sindreth Basin while Malani Igneous Suite is largely dominated by felsic volcanics and plutons, arguing against a delamination model (Sharma, 2005; van Lente et al., 2009). Similarly, convective thinning could result in diffusive and widespread volcanism, which is inconsistent with the spatially limited and linearly distributed basic rocks in the Sindreth and Punagarh basins (Fig. 1) (van Lente et al., 2009). Moreover, a progressive decrease in melting depth accompanied by transition from metasomatized lithospheric to asthenospheric mantle is expected in a convective thinning context (McKenzie and Bickle, 1988; Turner et al., 1999). The asthenospheric mantle melting for OIB-type Sindreth basalts is interpreted at a deeper level as compared to Punagarh *E*-MORB type basalt (Fig. 13), arguing against a convective thinning process.

The heterogeneous mantle sources inferred for the Sindreth and Punagarh basalts can be explained through slab break-off as the likely mechanism. Decompression melting of upwelling sub-slab asthenosphere through slab window facilitated interaction between asthenosphere derived magma and down moving sub-arc lithosphere, resulting in the generation of basaltic rocks with depleted MORB and enriched OIB-like geochemical signatures (Cole et al., 2006; D'Orazio et al., 2001; Gorring et al., 2003; Thorkelson et al., 2011). Therefore, the presence of E-MORB and OIB type basalts, as well as A-type volcanics, in Punagarh and Sindreth basins, can be explained through a slab break-off process. In this scenario, the Punagarh E-MORB type magma was generated by a relatively higher degree (~10–20%) of partial melting of this metasomatized mantle source at a shallow depth. In contrast, the Sindreth OIB-type basaltic melt was generated by a relatively lower degree (~5%) of partial melting of upwelling asthenosphere at a greater depth, further enriched by slab-derived fluids. The OIB-type volcanic rocks may be more resistant to melting during subduction than MORB-type, thus metasomatizing the mantle wedge at a depth greater than the source required for normal arc volcanoes (Zhou et al., 2012). Moreover, linear distribution and limited extent of mafic volcanic rocks in Sindreth and Punagarh basins are consistent with their narrow, linear zone and small volume as compared to oceanic island, plateau basalts and mafic magmas produced by slab break-off (Cole et al., 2006; Gorring et al., 2003; Tang et al., 2012; Xu et al., 2008).

The isotopically variable A-type felsic melts were generated by partial melting of both juvenile mafic crust and mature continental crust of the arc basement, which were heated by high heat flow resulting from upwelling asthenosphere and basaltic underplating. As discussed in the preceding sections, the A-type volcanic rocks have high Y/Nb and Yb/Ta ratios that are geochemically different from oceanic island basalts related to intraplate rifting but similar to continent-continent collision or island-arc magmatism. On the other hand, the 870–800 Ma Erinpura Granite in the NW India has been considered the product of convergence initiated by subducting oceanic plate (Just et al., 2011; Solanki, 2011) (Fig. 16a); the process that continued at least till 780–770 Ma (Ashwal et al., 2013; de Wall et al., 2012; Dharma Rao et al., 2012). Therefore, it seems more likely that the Sindreth and Punagarh volcanic rocks were generated in a convergent setting (Fig. 16b), notwithstanding the bimodal nature. The bimodal volcanism may not necessarily be a definitive indicator of continental rifting or plume-related regionally extensional settings, especially in case of small and dismembered geological entities (e.g. van Lente et al., 2009). There are several examples of present day and ancient convergent continental setting bimodal magmatism, such as the Villarrica-Lanin volcanic chain and Meseta del Lago Buenos Aires plateau in the Andes (D'Orazio et al., 2001; Hickey-Vargas et al., 1989) as well as Neoproterozoic bimodal volcanism in back-arc basin in the Yangtze Block of South China (Li et al., 2016).

5.6. Implications for paleoposition of NW India in Rodinia

MIS has been identified as a key segment in the reconstruction of the Rodinia supercontinent, as it forms part of a pulse of activity linking Madagascar, the Seychelles, NW India and South China. Their spatial position has been envisaged either at supercontinent peripheral or as a separate tectonic micro-plate off the supercontinent (Ashwal et al., 2002; Cawood et al., 2013, 2017; Merdith et al., 2017; T.H. Torsvik et al., 2001; Wang and Zhou, 2012; Yan et al., 2002; Zheng, 2004; Zhou et al., 2006). Moreover, petrogenetic models for MIS are varied and at times, contradictory (rift-related, A-type, plume- related, subduction- related and even associated with mantle delamination) and continue to be debated (Ashwal et al., 2013). Absence of large volume of mafic component refutes a mantle-plume driven origin for Malani magmatism. Structural elements and microstructural criteria, such as steep foliations, vertical lineations, dextral displacement, etc. observed in the ~765 Ma Mt. Abu batholith, spatially proximal to Sindreth Basin, indicate a transpressional setting (unclassified granites

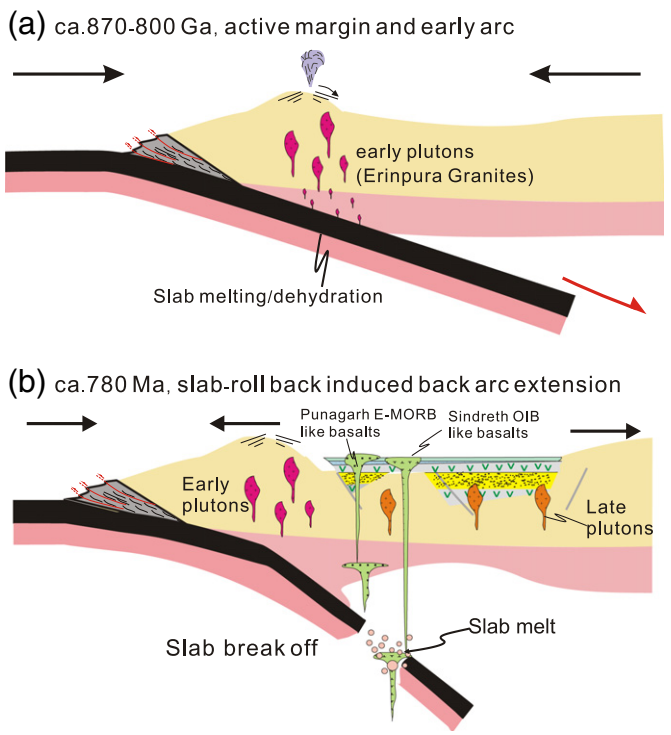

Fig. 16. Cartoon illustrating tectonic evolution in NW India during middle Neoproterozoic. (a) 870–800 Ma: oceanic plate subduction under the NW India leading to the generate early arc-related plutons, the 870–800 Ma Erinpura granitic rocks; (b) Slab-roll back induced back-arc extension and generation of variable types of basaltic magma due to upwelling asthenosphere through the slab window.

in Fig. 1c) (de Wall et al., 2012). The transpressional forces responsible for shaping the structural architecture in the Mt. Abu-Sirohi region were induced during closure of the Mozambique Ocean (de Wall et al., 2012). Therefore, an overall convergent continental margin setting for the NW India at 770–750 Ma is interpreted. The slab break-off model for generation of bimodal volcanics in the Sindreth and Punagarh basins is consistent with local structural geometry and does not support the continental rifting or plume setting. This interpretation envisages a convergent margin setting and paleoposition of NW India either along the periphery of Rodinia or off the Supercontinent with convergence and plate margin magmatism coinciding with the breakup of Rodinia.

6. Conclusions

Geochemical characteristics of Punagarh and Sindreth basalts underline chemically heterogeneous E-MORB and OIB type mantle sources, respectively. The primary magma for Punagarh basalts was derived from relatively shallow spinel facies mantle source whereas Sindreth basalts were sourced from a relatively deeper garnet bearing mantle source. Both the source regions were enriched by slab melts either from a previous or an ongoing subduction. Decompression melting of upwelling sub-slab asthenosphere through slab window facilitated interaction between asthenosphere derived magma and down moving sub-arc lithosphere, resulting in the generation of MORB- and OIB-like basalts. The associated felsic volcanics were derived from melting of continental crust that had been through a cycle of continent-continent collision or island-arc magmatism. A localized extension setting within an overall convergent background is inferred for Sindreth and Punagarh volcanics, and possibly, the MIS. Accordingly, the NW Indian block is inferred to occupy an external paleoposition in the Rodinia supercontinent assembly.

Supplementary data to this article can be found online at https://doi.org/10.1016/j.lithos.2017.11.010.

Acknowledgments

This study was supported by the National Natural Science Foundation of China (NSFC 41572170), "Thousand Youth Talents Plan" grants to Wei Wang and Wei-Terry Chen, the Belt and Road Initiatives (DL2017ZGDZ[*WH*]030) and MOST Special Fund from the State Key Laboratory of Geological Processes and Mineral Resources (MSFGPMR11 and 01-1). We would like to thank Dan Zhu for LA-ICPMS analyses, Abin Lin, Haihong Chen and Ping Xiao for whole rock elemental and isotopic analyses. Vivek Kumar Meena is thanked for his generous help during field work. We thank two anonymous reviewers for constructive comments and Prof. Nelson Eby for editorial handling and comments that helped in improving the manuscript.

References

Aldanmaz, E., Pearce, J.A., Thirlwall, M., Mitchell, J., 2000. Petrogenetic evolution of late Cenozoic, post-collision volcanism in western Anatolia, Turkey. Journal of Volcanology and Geothermal Research 102, 67–95.
Arndt, N.T., 1994. Archean komatiites. In: Condie, K.C. (Ed.), Archean Crustal Evolution. Elsevier, Amsterdam, pp. 11–44.
Ashwal, L., Demaiffe, D., Torsvik, T., 2002. Petrogenesis of Neoproterozoic granitoids and related rocks from the Seychelles: the case for an Andean-type arc origin. Journal of Petrology 43, 45–83.
Ashwal, L., Solanki, A., Pandit, M., Corfu, F., Hendriks, B., Burke, K., Torsvik, T., 2013. Geochronology and geochemistry of Neoproterozoic Mt. Abu granitoids, NW India: regional correlation and implications for Rodinia paleogeography. Precambrian Research 236, 265–281.
Bhushan, S.K., 2000. Malani rhyolites - a review. Gondwana Research 3, 65–77.
Cawood, P.A., Wang, Y.J., Xu, Y.J., Zhao, G.C., 2013. Locating South China in Rodinia and Gondwana: a fragment of greater India lithosphere? Geology 41, 903–906.
Cawood, P.A., Zhao, G.C., Yao, J.L., Wang, W., Xu, Y.J., Wang, Y.J., 2017. Reconstructing South China in Phanerozoic and Precambrian supercontinents. Earth Science Reviews https://doi.org/10.1016/j.earscirev.2017.06.001 (in press).
Chen, F.K., Siebel, W., Satir, M., Terzioglu, M., Saka, K., 2002. Geochronology of the Karadere basement (NW Turkey) and implications for the geological evolution of the Istanbul zone. International Journal of Earth Sciences 91, 469–481.
Chen, F.K., Li, X.H., Wang, X.L., Li, Q.L., Siebel, W., 2007. Zircon age and Nd-Hf isotopic composition of the Yunnan Tethyan belt, southwestern China. International Journal of Earth Sciences 96, 1179–1194.
Chore, S.A., Mohanty, M., 1998. Stratigraphy and tectonic setting of the Trans-Aravalli neoproterozoic volcanosedimentary sequences in Rajasthan. J. Geol. Soc. India 51, 57–68.
Choudhary, A.K., Gopalan, K., Sastry, C.A., 1984. Present status of the geochronology of the Precambrian rocks of Rajasthan. Tectonophysics 105, 131–140.
Clemens, J.D., Holloway, J.R., White, A.J.R., 1986. Origin of an A-type granite; experimental constraints. American Mineralogist 71, 317–324.
Cole, R.B., Nelson, S.W., Layer, P.W., Oswald, P.J., 2006. Eocene volcanism above a depleted mantle slab window in southern Alaska. Geological Society of America Bulletin 118, 140–158.
Collins, W.J., Beams, S.D., White, A.J.R., Chappell, B.W., 1982. Nature and origin of A-type granites with particular reference to southeastern Australia. Contributions to Mineralogy and Petrology 80, 189–200.
Collins, A.S., Clark, C., Plavsa, D., 2014. Peninsular India in Gondwana: the tectonothermal evolution of the southern granulite terrain and its Gondwanan counterparts. Gondwana Research 25, 190–203.
Condie, K.C., 1993. Chemical composition and evolution of the upper continental crust: contrasting results from surface samples and shales. Chemical Geology 104, 1–37.
Condie, K.C., 2003. Incompatible element ratios in oceanic basalts and komatiites: tracking deep mantle sources and continental growth rates with time. Geochemistry, Geophysics, Geosystems 4, 1–28.
de Wall, H., Pandit, M.K., Dotzler, R., Just, J., 2012. Cryogenian transpression and granite intrusion along the western margin of Rodinia (Mt. Abu region): magnetic fabric and geochemical inferences on Neoproterozoic geodynamics of the NW Indian block. Tectonophysics 554–557, 143–158.
de Wall, H., Pandit, M.K., Donhauser, I., Schöbel, S., Wang, W., Sharma, K.K., 2017. Evolution and tectonic setting of the Malani - Nagarparkar igneous suite: a Neoproterozoic silicic LIP in NW India-SE Pakistan. Journal of Asian Earth Sciences (in revision).
Deb, M., Thorpe, R.I., Krstic, D., Corfu, F., Davis, D.W., 2001. Zircon U-Pb and galena Pb isotope evidence for an approximate 1.0 Ga terrane constituting the western margin of the Aravalli-Delhi orogenic belt, northwestern India. Precambrian Research 108, 195–213.
DePaolo, D.J., 1981. Trace element and isotopic effects of combined wallrock assimilation and fractional crystallization. Earth and Planetary Science Letters 53, 189–202.
Dharma Rao, C.V., Santosh, M., Kim, S.W., 2012. Cryogenian volcanic arc in the NW Indian shield: zircon SHRIMP U–Pb geochronology of felsic tuffs and implications for Gondwana assembly. Gondwana Research 22, 36–53.
D'Orazio, M., Agostini, S., Innocenti, F., Haller, M.J., Manetti, P., Mazzarini, F., 2001. Slab window-related magmatism from southernmost South America: the late Miocene mafic volcanics from the Estancia Glencross area (~52°S, Argentina–Chile). Lithos 57, 67–89.

Eby, G.N., 1990. The A-type granitoids: a review of their occurrence and chemical characteristics and speculations on their petrogenesis. Lithos 26, 115–134.
Eby, G.N., 1992. Chemical subdivision of the A-type granitoids: petrogenetic and tectonic implications. Geology 20 (641–544).
Eby, G.N., Kochhar, N., 1990. Geochemistry and petrogenesis of the Malani igneous suite, north peninsular India. J. Geol. Soc. India 36, 109–130.
Evans, D.A.D., 2013. Reconstructing pre-Pangean supercontinents. Geological Society of America Bulletin 125, 1735–1751.
Gardien, V., Lardeaux, J.M., Ledru, P., Allemand, P., Guillot, S., 1997. Metamorphism during late orogenic extension: insights from the French Variscan belt. Bulletin de la Societe Geologique de France 168, 271–286.
Gorring, M., Singer, B., Gowers, J., Kay, S.M., 2003. Plio–Pleistocene basalts from the Meseta del Lago Buenos Aires, Argentina: evidence for asthenosphere–lithosphere interactions during slab window magmatism. Chemical Geology 193, 215–235.
Gregory, L.C., Meert, J.G., Bingen, B., Pandit, M.K., Torsvik, T.H., 2009. Paleomagnetism and geochronology of the Malani igneous suite, Northwest India: implications for the configuration of Rodinia and the assembly of Gondwana. Precambrian Research 170, 13–26.
Gupta, S., 1997. The Precambrian geology of the Aravalli region, southern Rajasthan and northeastern Gujarat. Geological Survey of India.
Heron, A.M., 1953. Geology of Central Rajputana. Geological Society of India, Bangalore, Memoirs, p. 79.
Hickey -Vargas, R., Roa, H.M., Escobar, L.L., Frey, F.A., 1989. Geochemical variations in Andean basaltic and silicic lavas from the Villarrica-Lanin volcanic chain (39.5° S): an evaluation of source heterogeneity, fractional crystallization and crustal assimilation. Contributions to Mineralogy and Petrology 103, 361–386.
Hoffman, P., 1991. Did the breakout of Laurentia turn Gondwanaland inside-out? Science 252, 1409.
Hoffman, P.F., Kaufman, A.J., Halverson, G.P., Schrag, D.P., 1998. A Neoproterozoic snowball earth. Science 281, 1342–1346.
Houseman, G.A., McKenzie, D.P., Molnar, P., 1981. Convective instability of a thickened boundary layer and its relevance for the thermal evolution of continental convergent belts. Journal of Geophysical Research - Solid Earth 86, 6115–6132.
Jiang, Y.-H., Ling, H.-F., Jiang, S.-Y., Fan, H.-H., Shen, W.-Z., Ni, P.E.I., 2005. Petrogenesis of a late Jurassic Peraluminous volcanic complex and its high-Mg, potassic, quenched enclaves at Xiangshan, Southeast China. Journal of Petrology 46, 1121–1154.
Jochum, K.P., Arndt, N.T., Hofmann, A.W., 1991. Nb-Th-La in komatiites and basalts: constraints on komatiite petrogenesis and mantle evolution. Earth and Planetary Science Letters 107, 272–289.
Just, J., Schulz, B., de Wall, H., Jourdan, F., Pandit, M.K., 2011. Monazite CHIME/EPMA dating of Erinpura granitoid deformation: implications for Neoproterozoic tectonothermal evolution of NW India. Gondwana Research 19, 402–412.
Kaur, P., Chaudhri, N., Raczek, I., Kroener, A., Hofmann, A.W., 2007. Geochemistry, zircon ages and whole-rock Nd isotopic systematics for Palaeoproterozoic A-type granitoids in the northern part of the Delhi belt, Rajasthan, NW India: implications for late Palaeoproterozoic crustal evolution of the Aravalli craton. Geological Magazine 144, 361–378.
Kepezhinskas, P., McDermott, F., Defant, M.J., Hochstaedter, A., Drummond, M.S., Hawkesworth, C.J., Koloskov, A., Maury, R.C., Bellon, H., 1997. Trace element and Sr-Nd-Pb isotopic constraints on a three-component model of Kamchatka Arc petrogenesis. Geochimica et Cosmochimica Acta 61, 577–600.
Kerrich, R., Polat, A., Wyman, D., Hollings, P., 1999. Trace element systematics of Mg-, to Fe-tholeiitic basalt suites of the Superior Province: implications for Archean mantle reservoirs and greenstone belt genesis. Lithos 46, 163–187.
Kochhar, N., 1984. Malani igneous suite: hot-spot magmatism and cratonization of the northern part of the Indian shield. Geological Society of India 25, 155–161.
Lahaye, Y., Arndt, N., 1996. Alteration of a komatiite flow from Alexo, Ontario, Canada. Journal of Petrology 37, 1261–1284.
Landenberger, B., Collins, W.J., 1996. Derivation of A-type granites from a dehydrated Charnockitic lower crust: evidence from the Chaelundi complex, Eastern Australia. Journal of Petrology 37, 145–170.
Le Roex, A.P., 1986. Geochemical Correlation between Southern African Kimberlites and South Atlantic Hotspots.
Li, Z.X., Bogdanova, S.V., Collins, A.S., Davidson, A., De Waele, B., Ernst, R., Fitzsimons, I., Fuck, R.A., Gladkochub, D.P., Jacobs, J., 2008. Assembly, configuration, and break-up history of Rodinia: a synthesis. Precambrian Research 160, 179–210.
Li, Z.X., Evans, D.A.D., Halverson, G.P., 2013. Neoproterozoic glaciations in a revised global palaeogeography from the breakup of Rodinia to the assembly of Gondwanaland. Sedimentary Geology 294, 219–232.
Li, L., Lin, S., Xing, G., Davis, D.W., Jiang, Y., Davis, W., Zhang, Y., 2016. Ca. 830 Ma back-arc type volcanic rocks in the eastern part of the Jiangnan orogen: implications for the Neoproterozoic tectonic evolution of South China Block. Precambrian Research 275, 209–224.
Liu, Y., Hu, Z., Zong, K., Gao, C., Gao, S., Xu, J., Chen, H., 2010. Reappraisement and refinement of zircon U-Pb isotope and trace element analyses by LA-ICP-MS. Chinese Science Bulletin 55, 1535–1546.
Loiselle, M.C., Wones, D.R., 1979. Characteristics and origin of anorogenic granites. Geological Society of America Abstract with Programs. 11, p. 468.
Ludwig, K.R., 2003. User's Manual for Isoplot 3.00, a Geolocronolgical Toolkit for Microsoft Excel. Berkeley: Berkeley Geochronlogical Center Special Publication 4 pp. 25–32.
McCall, G.J.H., 2006. The Vendian (Ediacaran) in the geological record: enigmas in geology's prelude to the Cambrian explosion. Earth-Science Reviews 77, 1–229.
McKenzie, D., Bickle, M.J., 1988. The volume and composition of melt generated by extension of the lithosphere. Journal of Petrology 29, 625–679.
McKenzie, D.A.N., O'Nions, R.K., 1991. Partial Melt Distributions from Inversion of Rare Earth Element Concentrations. Journal of Petrology 32, 1021–1091.
Meert, J.G., Lieberman, B.S., 2008. The Neoproterozoic assembly of Gondwana and its relationship to the Ediacaran–Cambrian radiation. Gondwana Research 14, 5–21.
Meert, J.G., Pandit, M.K., 2015. The Archaean and Proterozoic history of peninsular India: tectonic framework for Precambrian sedimentary basins in India. Geological Society, London, Memoirs 43, 29–54.
Meert, J.G., Pandit, M.K., Kamenov, G.D., 2013. Further geochronological and paleomagnetic constraints on Malani (and pre-Malani) magmatism in NW India. Tectonophysics 608, 1254–1267.
Merdith, A.S., Collins, A.S., Williams, S.E., Pisarevsky, S., Foden, J.F., Archibald, D., Blades, M.L., Alessio, B.L., Armistead, S., Plavsa, D., Clark, C., Müller, R.D., 2017. A full-plate global reconstruction of the Neoproterozoic. Gondwana Research https://doi.org/10.1016/j.gr.2017.04.001 (in press).
Meschede, M., 1986. A method of discriminating between different types of mid-ocean ridge basalts and continental tholeiites with the Nb-Zr-Y diagram. Chemical Geology 56, 207–218.
Moores, E., 1991. Southwest US-East Antarctic (SWEAT) connection: a hypothesis. Geology 19, 425–428.
Nance, R.D., Murphy, J.B., Santosh, M., 2014. The supercontinent cycle: a retrospective essay. Gondwana Research 25, 4–29.
Pandit, M.K., Carter, L.M., Ashwal, L.D., Tucker, R.D., Torsvik, T.H., Jamtveit, B., Bhushan, S.K., 2003. Age, petrogenesis and significance of 1.0 Ga granitoids and related rocks from the Sendra area, Aravalli Craton, NW India. Journal of Asian Earth Sciences 22, 363–381.
Pareek, H.S., 1981. Petrochemistry and Petrogenesis of the Malani Igneous Suite, India. Geological Society of America Bulletin 92, 206–273.
Pearce, J.A., 1983. Role of the sub-continental lithosphere in magma genesis at active continental margins. Continental Basalts & Mantle Xenoliths. 147, pp. 2162–2173.
Pearce, J., Peate, D., 1995. Tectonic implications of the composition of volcanic arc magmas. Annual Review of Earth and Planetary Sciences 23, 251–286.
Polat, A., Hofmann, A.W., Rosing, M.T., 2002. Boninite-like volcanic rocks in the 3.7–3.8 Ga Isua greenstone belt, West Greenland: geochemical evidence for intra-oceanic subduction zone processes in the early Earth. Chemical Geology 184, 231–254.
Robinson, J.A.C., Wood, B.J., 1998. The depth of the spinel to garnet transition at the peridotite solidus. Earth and Planetary Science Letters 164, 277–284.
Roy, A., Kröner, A., 1996. Single zircon evaporation ages constraining the growth of the Archaean Aravalli craton, northwestern Indian shield. Geological Magazine 133, 333–342.
Roy, A.B., Jakhar, S.R, 2002. Geology of Rajasthan: Precambrian to Recent. Scientific Publishers (India), Jodhpur 421p.
Rudnick, R., Gao, S., 2003. Composition of the continental crust. Treatise on Geochemistry. 3, pp. 1–64.
Schöbel, S., Sharma, K.K., Hörbrand, T., Böhm, T., Dönhauser, I., de Wall, H., 2017. Continental rift setting and evolution of Neoproterozoic Sindreth Basin in NW India. Journal of Earth System Science https://doi.org/10.1007/s12040-017-0855-6.
Sharma, K.K., 2004. The Neoproterozoic Malani magmatism of the northwestern Indian shield: implications for crust-building processes. Journal of Earth System Science 113, 795–807.
Sharma, K.K., 2005. Malani magmatism: an extensional lithospheric tectonic origin. Geological Society of America Special Papers 388, 463–476.
Shervais, J.W., 1982. Ti-V plots and the petrogenesis of modern and ophiolitic lavas. Earth and Planetary Science Letters 59, 101–118.
Shields, G.A., 2007. A normalised seawater strontium isotope curve: possible implications for Neoproterozoic-Cambrian weathering rates and the further oxygenation of the Earth. eEarth 2, 35–42.
Siddiqui, R.H., Ma, C., 2017. Petrogenesis of late cretaceous volcanism in Kazhaba area and its relationship with mantle plume activity of Reunion hotspot. Journal of Earth Science 28, 229–240.
Sinha-Roy, S., Malhotra, G., Mohanty, M., 1998. Geology of Rajasthan. Geological Society of India, Bangalore.
Solanki, A.M., 2011. A Petrographic, Geochemical and Geochronological Investigation of Deformed Granitoids from SW Rajasthan: Neoproterozoic Age of Formation and Evidence of Pan-African Imprint. University of the Witwatersrand Johannesburg, p. 216.
Spencer, C.J., Hawkesworth, C., Cawood, P.A., Dhuime, B., 2013. Not all supercontinents are created equal: Gondwana-Rodinia case study. Geology 41, 795–798.
Sun, S.S., McDonough, W.F., 1989. Chemical and isotopic systematics of oceanic basalts: implications for mantle composition and processes. Geological Society, London, Special Publications 42, 313–345.
Tang, G.-J., Wyman, D.A., Wang, Q., Li, J., Li, Z.-X., Zhao, Z.-H., Sun, W.-D., 2012. Asthenosphere–lithosphere interaction triggered by a slab window during ridge subduction: trace element and Sr–Nd–Hf–Os isotopic evidence from late carboniferous tholeiites in the western Junggar area (NW China). Earth and Planetary Science Letters 329–330, 84–96.
Taylor, S., McLennan, S., 1985. The Continental Crust: Its Composition and Evolution. Oxford Blackwell, p. 311.
Thorkelson, D.J., Madsen, J.K., Sluggett, C.L., 2011. Mantle flow through the Northern Cordilleran slab window revealed by volcanic geochemistry. Geology 39, 267–270.
Torsvik, T., Ashwal, L., Tucker, R., Eide, E., 2001a. Neoproterozoic geochronology and palaeogeography of the Seychelles microcontinent: the India link. Precambrian Research 110, 47–59.
Torsvik, T.H., Carter, L.M., Ashwal, L.D., Bhushan, S.K., Pandit, M.K., Jamtveit, B., 2001b. Rodinia refined or obscured: palaeomagnetism of the Malani igneous suite (NW India). Precambrian Research 108, 319–333.

Turner, S.P., Foden, J.D., Morrison, R.S., 1992. Derivation of some A-type magmas by fractionation of basaltic magma: an example from the Padthaway Ridge, South Australia. Lithos 28, 151–179.
Turner, S.P., Platt, J.P., George, R.M.M., Kelley, S.P., Pearson, D.G., Nowell, G.M., 1999. Magmatism associated with orogenic collapse of the Betic–Alboran domain, SE Spain. Journal of Petrology 40, 1011–1036.
van Lente, B., Ashwal, L., Pandit, M., Bowring, S., Torsvik, T., 2009. Neoproterozoic hydrothermally altered basaltic rocks from Rajasthan, northwest India: implications for late Precambrian tectonic evolution of the Aravalli Craton. Precambrian Research 170, 202–222.
Vijaya Rao, V., Krishna, V.G., 2013. Evidence for the Neoproterozoic Phulad suture zone and genesis of Malani magmatism in the NW India from deep seismic images: implications for assembly and breakup of the Rodinia. Tectonophysics 589, 172–185.
von Blanckenburg, F., Davies, J.H., 1995. Slab breakoff: a model for syncollisional magmatism and tectonics in the Alps. Tectonics 14, 120–131.
Wang, W., Zhou, M.F., 2012. Sedimentary records of the Yangtze Block (South China) and their correlation with equivalent Neoproterozoic sequences on adjacent continents. Sedimentary Geology 265–266, 126–142.
Wang, W., Cawood, P.A., Zhou, M.F., Pandit, M.K., Chen, W.T., 2017a. Zircon U-Pb age and Hf isotope evidence for Eoarchean crustal remnant, and crustal growth and reworking respond to supercontinental cycles in NW India. Journal of Geological Society 174, 759–772.
Wang, W., Cawood, P.A., Zhou, M.F., Pandit, M.K., Xia, X.P., Zhao, J.H., 2017b. Low-$\delta^{18}O$ rhyolites from the Malani Igneous Suite: a positive test for South China and NW India linkage in Rodinia. Geophysical Research Letters 44, 10298–10305.
Whalen, J.B., Currie, K.L., Chappell, B.W., 1987. A-type granites: geochemical characteristics, discrimination and petrogenesis. Contributions to Mineralogy and Petrology 95, 407–419.
Wiedenbeck, M., Goswami, J.N., 1994. High precision $^{207}Pb/^{206}Pb$ zircon geochronology using a small ion microprobe. Geochimica et Cosmochimica Acta 58, 2135–2141.
Winchester, J.A., Floyd, P.A., 1976. Geochemical magma type discrimination: application to altered and metamorphosed basic igneous rocks. Earth and Planetary Science Letters 28, 459–469.
Xu, Y.G., Lan, J.B., Yang, Q.J., Huang, X.L., Qiu, H.N., 2008. Eocene break-off of the Neo-Tethyan slab as inferred from intraplate-type mafic dykes in the Gaoligong orogenic belt, eastern Tibet. Chemical Geology 255, 439–453.
Yan, D.P., Zhou, M.F., Song, H.L., Malpas, J., 2002. Where was South China located in the reconstruction of Rodinia. Earth Science Frontiers 9, 249–256 (in Chinese with English abstract).
Zhang, X.B., Wang, K.Y., Wang, C.Y., Li, W., Yu, Q., Wang, Y.C., Li, J.F., Wan, D., Huang, G.H., 2017. Age, genesis, and tectonic setting of the Mo-W mineralized Dongshanwan granite porphyry from the Xilamulun metallo-genic belt, NE China. Journal of Earth Science https://doi.org/10.1007/s12583-016-0934-1 (in press).
Zhao, X.F., Zhou, M.F., Li, J.W., Wu, F.Y., 2008. Association of Neoproterozoic A-and I-type granites in South China: implications for generation of A-type granites in a subduction-related environment. Chemical Geology 257, 1–15.
Zheng, Y.F., 2004. Position of South China in configuration of Neoproterozoic supercontinent. Chinese Science Bulletin 49, 751–753.
Zhou, M.F., Yan, D.P., Wang, C.L., Qi, L., Kennedy, A., 2006. Subduction-related origin of the 750 Ma Xuelongbao adakitic complex (Sichuan Province, China): implications for the tectonic setting of the giant Neoproterozoic magmatic event in South China. Earth and Planetary Science Letters 248, 286–300.
Zhou, M.F., Robinson, P.T., Wang, C.Y., Zhao, J.H., Yan, D.P., Gao, J.F., Malpas, J., 2012. Heterogeneous mantle source and magma differentiation of quaternary arc-like volcanic rocks from Tengchong, SE margin of the Tibetan Plateau. Contributions to Mineralogy and Petrology 163, 841–860.